Bioorganic Chemistry 85 (2019) 585–599

Contents lists available at ScienceDirect

Bioorganic Chemistry

journal homepage: www.elsevier.com/locate/bioorg

Design, synthesis, and DNA interaction studies of furo-imidazo[3.3.3] propellane derivatives: Potential anticancer agents

Alaa A. Hassan[a,*], Ashraf A. Aly[a], Nasr K. Mohamed[a], Kamal M. El Shaieb[a], Maysa M. Makhlouf[a], El-Shimaa M.N. Abdelhafez[b], Stefan Bräse[c,d], Martin Nieger[e], Kevin N. Dalby[f], Tamer S. Kaoud[b,f,*]

[a] Chemistry Department, Faculty of Science, Minia University, El-Minia 61519, Egypt
[b] Department of Medicinal Chemistry, Faculty of Pharmacy, Minia University, El-Minia 61519, Egypt
[c] Institute of Organic Chemistry, Karlsruhe Institute of Technology, Fritz-Haber-Weg 6, Karlsruhe 76131, Germany
[d] Institute of Toxicology and Genetics, Hermann-von-Helmholtz-Platz 1, D-76344 Eggenstein-Leopoldshafen, Germany
[e] Department of Chemistry, University of Helsinki, P.O. Box 55, A.I. Virtasen aukio I, Helsinki 00014, Finland
[f] Division of Chemical Biology and Medicinal Chemistry, The University of Texas at Austin, Austin, TX 78712, USA

ARTICLE INFO

Keywords:
Furo-imidazo[3.3.3]-propellanes
Alkenylidene-hydrazinecarbothioamides
Dicyanomethylene-1,3-indanedione
DNA non-intercalative interaction
DNA damage induction
Non-small cell lung cancer

ABSTRACT

A large number of natural products containing the propellane scaffold have been reported to exhibit cytotoxicity against several cancers; however, their mechanism of action is still unknown. Anticancer drugs targeting DNA are mainly composed of small planar molecule/s that can interact with the DNA helix, causing DNA malfunction and cell death. The aim of this study was to design and synthesize propellane derivatives that can act as DNA intercalators and/or groove binders. The unique structure of the propellane derivatives and their ability to display planar ligands with numerous possible geometries, renders them potential starting points to design new drugs targeting DNA in cancer cells. New substituted furo-imidazo[3.3.3]propellanes were synthesized *via* the reaction of substituted alkenylidene-hydrazinecarbothioamides with 2-(1,3-dioxo-2,3-dihydro-1*H*-2-ylidene) propanedinitrile in tetrahydrofuran at room temperature. The structures of the products were confirmed by a combination of elemental analysis, NMR, ESI-MS, IR and single crystal X-ray analysis. Interestingly, **5c**, **5d** and **5f** showed an ability to interact with Calf Thymus DNA (CT-DNA). Their DNA-binding mode was investigated using a combination of absorption spectroscopy, DNA melting, viscosity, CD spectroscopy measurements, as well as competitive binding studies with several dyes. Their cytotoxicity was evaluated against the NCI-60 panel of cancer cell lines. **5c**, **5d** and **5f** exhibited similar anti-proliferative activity against the A549 non-small cell lung cancer (NSCLC) cell line. Further mechanistic studies revealed their ability to induce DNA damage in the A549 cell line, as well as apoptosis, evidenced by elevated Annexin V expression, enhanced caspase 3/7 activation and PARP cleavage. In this study, we present the potential for designing novel propellanes to provoke cytotoxic activity, likely through DNA binding-induced DNA damage and apoptosis.

1. Introduction

Propellanes are tricyclic entities with a central single bond surrounded by three small to medium rings. Since their discovery 53 years ago, their unusual structure has initiated a great interest in many fields, especially in life sciences because of their presence in several natural products and their various biological activities [1]. Although, there are over 10,000 representatives of this chemical class, new propellane-containing natural products still being discovered, with unique structures and activity profiles [1]. Several propellanes exhibiting antiviral [2], antifungal [3], antibiotic [4,5] and anticancer [6–9] activities have been previously described. For example, Dichrocephone B, that was isolated from *Dichrocephala benthamii*, contains a [3.3.3] propellane core structure fused to a unique oxetane ring (Fig. 1A), exhibits significant cytotoxicity against human oral squamous carcinoma cells (KB), human cervical cancer cells (HeLa), and non-small-cell lung carcinoma cells (A549), with IC_{50} values of 3.3, 4.1, and 4.5 μM, respectively [8]. Diepoxin δ which was isolated from the fungus *Nattrassia Mangiferae* (Fig. 1B) inhibits the ability of human fibrosarcoma cells (HT1080) to invade through a matrigel membrane with an IC_{50} of 0.75 μM [7]. Another example of propellanes with unique structures are Epicochalasines A and B, they were isolated from the liquid culture

* Corresponding authors at: Chemistry Department, Faculty of Science, Minia University, El-Minia 61519, Egypt (A.A. Hassan) and Division of Chemical Biology and Medicinal Chemistry, The University of Texas at Austin, Austin, TX 78712, USA (T.S. Kaoud).
E-mail addresses: alaahassan2001@mu.edu.eg (A.A. Hassan), tkaood1@utexas.edu (T.S. Kaoud).

https://doi.org/10.1016/j.bioorg.2019.02.027
Received 3 January 2019; Received in revised form 10 February 2019; Accepted 11 February 2019
Available online 13 February 2019

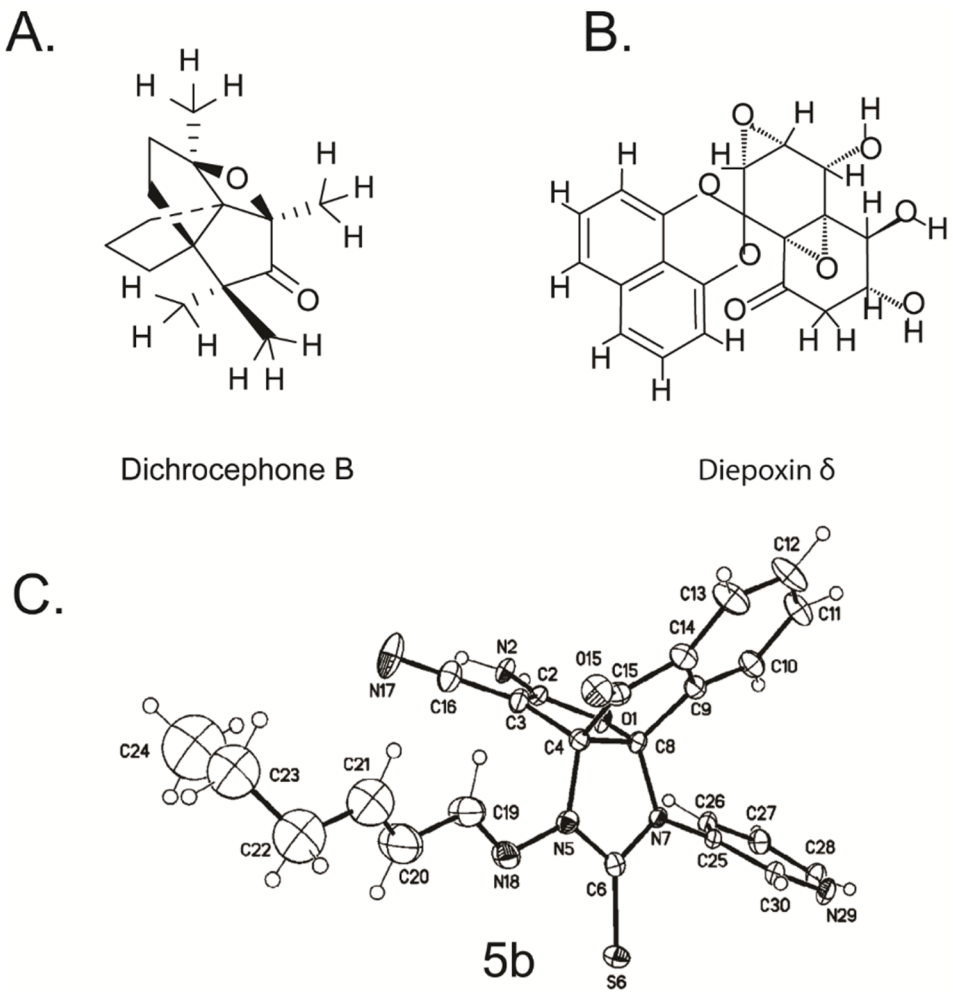

Fig. 1. Molecular structure of the propellane derivatives Dichrocephone B (A) and Diepoxin δ (B), reported to exhibit cytotoxic activity against several cancers [7,8]. (C) The crystal structure of the new propellane derivative 5b.

broth of the fungus *Aspergillus flavipes*. Their structures have both an adamantane-like structure, as well as a [4.4.3] propellane moiety with 19 stereogenic centers. These compounds have been reported to induce cell cycle arrest in an HL60 leukemia cell line and apoptosis in both HL60 and NB4 leukemia cell lines [9]. Although there are several reports of propellane natural products with considerable cytotoxicity and antitumor activities, little is known about their mechanism of action or their actual targets in cancer cells [1].

DNA is a major target of various anticancer drug discovery efforts [10]. Interaction of small planar aromatic or heteroaromatic molecules with DNA in cancer cells, may cause lengthening, stiffening or unwinding of the DNA helix, inhibit DNA replication, induce DNA damage [11,12] and block cell division which finally can lead to cell death [13]. Generally, drug-DNA interaction occurs through three possible non-covalent modes: intercalation, groove binding and external electrostatic effects. Intercalators bind reversibly by inserting a planar aromatic pharmacophore between adjacent base pairs of double-stranded DNA, which in turn can lead to antitumor activity [14,15]. For example, the metallo-intercalators contain planar, positively charged, polycyclic aromatic ligands [16]. They bind DNA through insertion between the planar bases [17]. Several metallo-intercalators are already used as cancer therapeutics including cisplatin, carboplatin, oxaliplatin and nedaplatin [18]. In the same time, targeting the DNA minor groove can be less challenging, the small width of the groove stabilizes the binding by providing several van der Waal's interactions and/or hydrogen bonding with the nucleobases [19]. Interestingly, several natural products have been known to bind the DNA minor groove, including chromomycin, actinomycin D, distamycin, netropsin, and Hoechst 33258 [20,21].

Here we hypothesis that propellane derivatives designed to carry planar aromatic or non-aromatic ligands can potentially act as DNA intercalators or minor groove binders with promising anti-tumor activity. Several methods are reported for the synthesis of heterocylic [3.3.3]propellanes. Oxa-aza[3.3.3]propellanes were synthesized by Alizadeh et al. [4,22–24], Yavari et al. [25], Chen et al. [26] and Zhang et al. [27]. Hassan et al. reported the formation of oxaaza- and bis-oxathia-aza[3.3.3]-propellanes *via* nucleophilic addition of symmetrical and unsymmetrical N^1,N^2-disubstituted-1,2-dicarbothioamides on dicyanomethylene-1,3-indanedione **1** [28]. The reaction of *N*,*N*,*N″*-(1,ω-alkandiyl)bis-(*N″*-organylthioureas) with **1** afforded new bis-oxathia-aza[3.3.3]propellanes [29].

Due to our continuous interest in the design and synthesis of new heterocycles with antitumor activity [30,31], in this study we synthesized a new group of hetero[3.3.3]propellanes by reacting heteroyl-hydrazinecarbothioamides with **1** to give furo-imidazo[3.3.3]propellanes [32]. Also, nucleophilic addition of thiocarbohydrazide derivatives with **1** gave furo-imidazo[3.3.3]propellanes [33]. The ability of the new compounds to interact with DNA was examined using several biophysical and biochemical techniques. The cytotoxicity of the compounds towards the NCI-60 panel of cancer cell lines was determined. And the molecular mechanism of three of the new derivatives was further investigated in the A549 non-small cell lung cancer cell line.

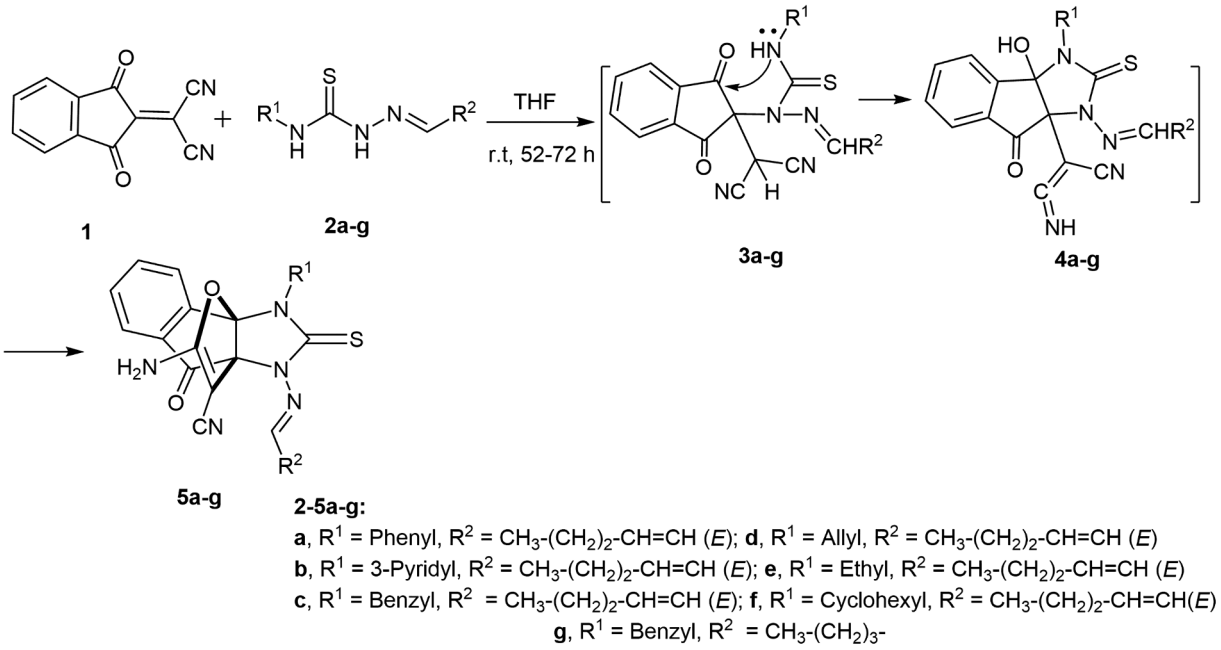

Scheme 1. Reactions of 1 with 2a–g in THF at room temperature, showing the mechanism of formation of furo-imidazo[3.3.3]propellanes 5a–g.

2. Results and discussion

2.1. Chemistry

The main purpose of this project was to design a new group of DNA-targeting small molecules using the propellane scaffold. The propellane should provide planar, polyaromatic ligands with enough hydrophobicity to extend into the base-stack of the DNA and/or fit into the DNA minor groove. (Fig. 1 and Scheme 1).

In order to synthesize such derivatives, initially we investigated the reactions of substituted (ylidenehydrazinecarbothioamides) **2a–g** bearing a selection of aryl, alkyl, alkenyl and heterocyclic substituents with **1** (Scheme 1). Under room temperature and atmospheric air, a mixture of dicyanomethylene-1,3-indanedione (**1**, 1.25 mmol) and alkenylidene-hydrazinecarbothioamides (**2a–g**, 1.0 mmol) was stirred in THF for 52–72 hrs. TLC analysis suggested the complete disappearance of compounds **1** and **2**. We found that furo-imidazo[3.3.3]propellanes **5a–g** were obtained as a colourless crystals in 71–84% yields.

The mass spectrum of **5b**, as an example displayed the molecular ion peak at m/z = 456 (11%), which is in agreement with the proposed structure and shows clearly the addition of one molecule of **2b** to one molecule of **1** without any elimination. The IR spectrum of **5b** in KBr shows a broad band at 3443–3400 cm^{-1} due to the NH_2 group, sharp bands at 2196 and 1728 cm^{-1}, characteristic of a conjugated nitrile and indeno-CO group, respectively. Two absorption bands at 1371 and 987 cm^{-1} (C═S and C—N str.) were observed as well as a characteristic band for C—O—C at 1102 cm^{-1}. The ^{1}H NMR spectrum of **5b**, exhibited a broad exchangeable signal with two protons at 8.50–8.52 ppm due to the NH_2 group. A triplet at 0.92–0.96 ppm due to the CH_3 group with coupling constant (J = 7.61 Hz). Two upfield multiplets at 1.48–1.54 and 2.28–2.31 are due to CH_2-CH_2, whereas a downfield multiplet at 6.36–6.39 corresponds to CH═CH, as well as to the aromatic protons. In the ^{13}C NMR spectrum of **5b** signals at 189.81, 178.93, and 154.06 are due to indeno-CO, thioxo and CH═N groups, respectively. Two peaks at δc = 49.58 (furan-C3), and 168.17 (furan-C2) are in accordance with the observed trends in δ values for carbon atoms in 'push-pull' alkenes [34,35]. Further signals at 81.45 (furan-C4), 103.86 (furan-C5), 110.0 and 115.70 (CH═CH). Three signals at 13.46, 21.24 and 34.32 correspond to the $CH_3CH_2CH_2$ moiety.

As it is difficult to assess the correct structure based on the NMR spectral data, the structure of these compounds was unequivocally resolved by single crystal X-ray analysis. Specifically, the structure of 2-amino-11((1*E*, 2*E*)-hex-2-en-1-ylidene)-amino)-4-oxo-9-(pyridyl-3-yl)-10-thioxo-4*H*-3*a*,8*b*-(epiminomethanoimino)-indeno[1,2-*b*]furan-3-carbonitrile (**5b**) was established unambiguously by single crystal X-ray analysis, which confirmed the presence of a propellane system (Fig. 1C and Tables S1–S7 in the supporting information). The X-ray crystal structure of **5b** clearly shows that the (C4)-(C8) bond length of 1.536 (4) Å has a C—C single bond character and is shared by three different rings C4-C8-N7-C6-N5, C4-C8-O1-C2-C3 and C4-C8-C9-C4-C15. The bond length C(6)-S(6) = 1.658 (3) Å and has C═S (1.645 Å) double bond character. The sums of the angles around C(4) and C(8) are 319° and 337°, respectively revealing that restrained around C4 and C8.

Compounds **2a–g** may react either with their sulphur atom, N^2 or N^4 as nucleophilic sites. On the other hand, it has been reported that the methine carbon of **2a–g** had to act as a nucleophile in the sense of an "umpolung" [36]. Thus, several options for interaction between **1** and **2a–g** may be expected. It is probable that the products **5a–g** are formed from one of the four labile 1:1 adducts. Several alternative structures can be suggested (Fig. 2), but some of these were ruled out based on the ^{13}C NMR spectral data. Comparison of the ^{1}H and ^{13}C NMR for the isomers **5–8** showed that propellanes **6** and **7** (Fig. 2) could be ruled out. Therefore, X-ray analysis may serve as a useful supplementary tool in determining the correct structure, and confirm that we have the propellane-type structures **5a–g** rather than **8a–g.**

It was found that the reaction conditions such as solvent, catalyst, temperature play an important role on the reaction efficiency. Different solvents were investigated, and it was found that tetrahydrofuran (THF) was superior compared to chlorobenzene, acetonitrile, dichloromethane and DMF. The effect of different basic media was investigated. THF without any additions showed high activity, while others such as EtOH/$(Et)_3$N and EtOH/piperidine were less effective. Increasing the amount of **1** to 1.5 mmol or 2 mmol led to a lower yield. High product yield was obtained in the presence of air. Only trace amounts of product were formed when the reaction was performed under nitrogen or argon. The reaction was carried out at different temperatures with THF as the solvent, but low product conversions were observed. Using alkenylidene-hydrazinecarbothioamides with benzyl, allyl, pyridyl and phenyl derivatives, the observed products **5a–g** were generated in 71–84% yields. These results indicate that both

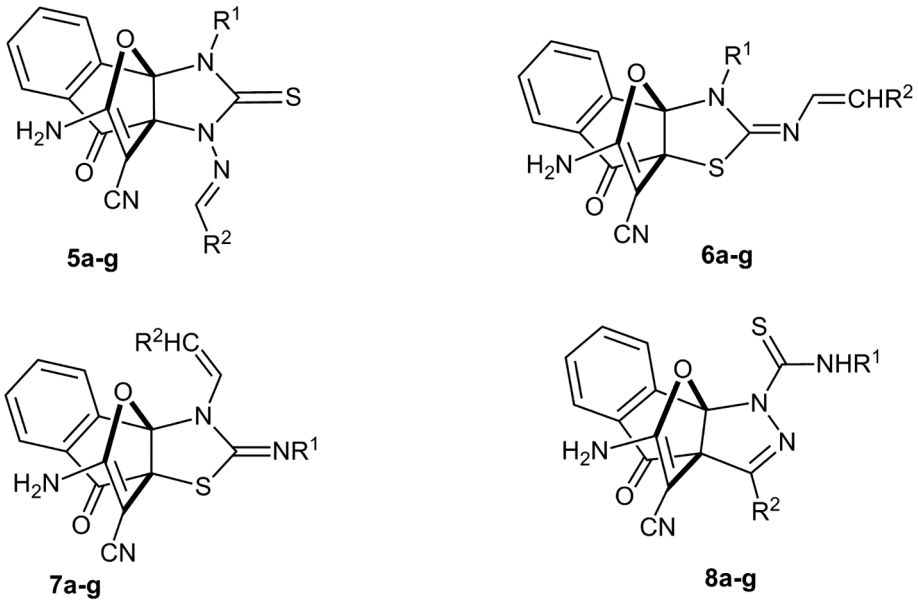

Fig. 2. Structures of possible isomers of compound 5.

electronic and steric factors have no significant influence on the efficiency of the reaction. To rationalize the formation of propellanes **5a–g** as depicted in scheme 1. The attack of the ^{2}NH group of **2a–g** on the C═C double bond of **1** affords the adduct **4a–g** *via* intermediate **3a–g**. Intramolecular nucleophilic attack of the OH on the imino group, affords furo-imidazo[3.3.3]propellanes **5a–g** (Scheme 1).

2.2. Biological investigation

2.2.1. Anti-proliferative investigation against 60 cancer cell lines at the National Cancer Institute (NCI), USA.

The selected compounds were subjected to *in vitro* anticancer assays against tumor cells in a full panel of 60 cell lines derived from nine different cancer types (leukemia, lung, colon, CNS, melanoma, ovarian, renal, prostate and breast cancers). The compounds were added at single concentration of 10^{-5} M and the culture was incubated for 48 h. Growth inhibition percent is illustrated in Table 1 and Table S9. **5a**, **5b**, **5e** and **5g** exhibited less anticancer activities (As shown in the supporting information, Table S8) if compared to **5c**, **5d** and **5f** (Shown down in Table 1).

As shown in Table 1, Compound **5c** exhibited the best activity against renal ACHN cell line with percentage growth inhibition of 73%, whereas, it revealed moderate activity (≥40% inhibition) against leukemia CCRF-CEM & RPMI-8226, Non-Small Cell Lung Cancer EKVX, A549 and NCI-H522, colon cancer HCT-116, prostate cancer PC-3, Melanoma M-14, renal cancer UO-31 and breast cancer cell lines MCF7 & T-47D. Compound **5f** (Table 1) showed inhibition activity against most cell lines, however, it exhibited significant inhibition against prostate PC-3, colon HT29, renal UO-31 and breast MCF7 cell lines with 77, 64, 62 and 70% inhibition respectively. **5f** inhibited the growth of the leukemia cell lines (K-562 and RPMI-8226), the non-small cell lung cancer cell lines (A549), the colon cancer cell line (HCT-116) and the breast cancer cell line (T-47D) with % inhibition > 40%. Also, **5d** (Table 1) showed moderate to mild inhibition activity (> 30% inhibition) against the non-small cell lung cancer cell line NCI-H522, the renal cancer cell line UO-31 and the breast cancer cell lines MCF-7 and T47-D.

On the other hand, Compound **5g** (Supporting information Table S8) revealed relatively the highest growth inhibitory activity against leukemia K-562 cell line with 87% growth inhibition. On the other hand, compounds **5a, 5b** and **5e** exhibited mild to weak activity against most tested cell lines (Supporting information Table S8). From these results we can conclude that the presence of benzyl or cyclohexyl group would enhance the anti-proliferative activity especially upon increasing the flexibility of the compound (as in compounds **5c** and **3f**), this extension increased the potency of these compounds against most tested cells. Compounds containing phenyl, ethyl and pyridyl groups did not exhibit remarkable anti-proliferative activity.

According to the screening results, we decided to go further and examine the capability of compounds **5c**, **5d** and **5f** to bind Calf Thymus DNA (CT-DNA) under physiological conditions.

2.2.2. DNA interaction studies

To test our hypothesis that the anticancer activity of propellane derivatives can be attributed to its ability to interact with DNA, several experiments were performed to test the interaction and characterize the possible binding mode (Table 2).

2.2.2.1. UV–Vis spectroscopy. Absorption spectroscopy is one of several techniques used to assess DNA-ligand binding, which results in double helix conformational changes that lead to UV spectrum alteration [37]. The interaction of any ligand with a DNA helix may result in a hyperchromic or hypochromic effect, as well as a red or blue shift. The absorbance spectra of a buffered solution of **5c**, **5d** or **5f** with different concentrations of Calf Thymus DNA (CT-DNA) revealed a consistent hypochromic effect over the 300–340 nm range, without any significant red or blue shift (Fig. 3A–C). Cheng-Yong et al, reported that the breaking of the DNA secondary structure that accompanies helix axis contraction is expected to produce a hyperchromic effect, while hypochromic effects can result from secondary structure stabilization by intercalation or groove binding [38]. In addition, Lafayette et al. and others have suggested that a combination of both a red shift and a hypochromic effect is indicative of an intercalation. Thus, a hypochromic effect in the absence of any red/blue shift, as seen with the propellane derivatives **5c**, **5d** and **5f**, suggests the possibility of a non-intercalative binding mechanism (e.g. groove binding), rather than intercalation [39–41].

Based on these UV–vis titration curves (Fig. 3A–C), the binding constants (K_a) and the n parameter, were calculated by fitting the absorption titration at 315 nm to the neighbor exclusion model of McGhee and von Hippel [42,43] (as described in the methods section). As another evidence of a non-intercalative binding mode, the scatchard plots

Table 1
% Growth inhibition of compounds 5c, 5d and 5f.

Panel/Cell Line	% Growth inhibition			Panel/Cell Line	% Growth inhibition		
	Compound				Compound		
	5c	5d	5f		5c	5d	5f
Leukemia				**Melanoma**			
CCRF-CEM	40.64	−0.22	20.48	LOX IMVI	25.61	5.8	10.87
HL-60 (TB)	29.58	1.34	38.21	MALME-3M	4.81	−4.03	5.73
K-562	32.42	7.18	50.66	M14	40.08	7.13	24.61
MOLT-4	38.9	11.42	34.78	MDA-MB-435	24.92	5.38	22.95
RPMI-8226	48.96	19.75	44.48	SK-MEL-2	10.03	−6.35	0.73
SR	11.28	1.58	39.13	SK-MEL-28	8.57	−10.44	5.82
Non-Small Cell Lung Cancer				SK-MEL-5	29.89	1.76	31.01
A549/ATCC	39.14	11.24	45.14	UACC-257	2.92	1.42	30.59
EKVX	45.94	17.74	13.24	UACC-62	33.69	15.86	28.42
HOP-62	29.11	15.01	2.89	**Ovarian Cancer**			
HOP-92	21.85	17.02	16.19	IGROV1	19	−5.64	1.44
NCI-H226	37.29	1.65	15.64	OVCAR-3	—	1.23	18.03
NCI-H23	21.39	5.79	6.86	OVCAR-4	28.3	6.36	21.38
NCI-H322M	15.54	8.05	−0.13	OVCAR-5	15.26	−0.62	7.95
NCI-H460	22.73	−6.31	38.84	OVCAR-8	20.76	6.85	37.13
NCI-H522	43.07	40.92	4.23	NCI/ADR-RES	19.47	−3.89	5.59
Colon Cancer				SK-OV-3	18.61	11.82	1.64
COLO 205	6.67	−14.94	28.99	**Renal Cancer**			
HCC-2998	6.4	−9.24	14.04	786-0	25.18	2.86	12.87
HCT-116	48.8	5.9	48.64	A498	15.07	15.4	16.67
HCT-15	38.9	18.27	31.67	ACHN	72.83	4.67	6.49
HT29	31.43	17.77	63.81	CAKI-1	———	———	———
KM12	———	−1.93	32.87	RXF 393	28.4	−2.11	25.4
SW-620	2.92	−11.86	21.43	SN12C	11.57	3.69	31.97
CNS Cancer				TK-10	3.2	−12.49	10.36
SF-268	———	5.69	8.88	UO-31	54.99	38.03	61.91
SF-295	33.22	11.51	34.62	**Breast Cancer**			
SF-539	11.92	2.56	0.75	MCF7	57.57	32.37	70.28
SNB-19	5.7	0.31	22.56	MDA-MB-231	25.7	10.27	11.47
SNB-75	34.78	29.2	9.78	HS 578T	20.95	4.66	21.21
U251	27.74	0.31	37.8	BT-549	27.92	17.36	22.29
Prostate Cancer				T-47D	55.67	33.16	51.28
PC-3	52.88	19.04	77.28	MDA-MB-468	30.96	−3	12.66
DU-31	———	−3.61	13.84				

(r/C_f vs r) of the three compounds (Fig. 3D–F) exhibited downward curvature, suggesting the binding of a single molecule along the DNA polymer without any other nearby ligand, a phenomenon that is also referred to as neighbor exclusion [42,43]. The association constant K_a as well as the n-parameter were calculated using the Scatchard plot analysis (Fig. 3D–F). As shown in Table 2, 5c and 5f showed 3–4 fold higher affinity than **5d** towards CT-DNA with $K_a = 0.39 \times 10^5$, 0.3×10^5 and $0.1 \times 10^5\ M^{-1}$ and n of ~26, 26 and 31 respectively, the observation that can be attributed to the hydrophobicity of the benzyl gp in **5c** and cyclohexyl gp in **5f** if compared to the allyl substituent in 5d (Scheme 1).

2.2.2.2. Thermal melting studies. Thermal denaturation experiments were performed to further assess the effect of the ligand binding on the CT-DNA helix conformation. DNA melting temperature (T_m) is the temperature at which half of the DNA denatures or becomes unwound. Intercalation into the helix is known to elevate this temperature by 5–8 °C due to the enhanced helix stability. While, the other binding modes (non-intercalative) as groove or electrostatic binding cause a limited changes in the DNA melting temperature [44–47]. Denaturation of the helix was monitored by following the UV absorbance of the CT-DNA at 260 nm as a function of the temperature. Results shown in Fig. 4, revealed that the three propellane derivatives **5c**, **5d** and **5f** similarly affected the CT-DNA double helix with limited changes in the melting temperature ΔT_m of 2.18, 1.93 and 1.92 °C respectively (Table 2) [37,48]. The results that provide further evidence for the suggested non-intercalative binding mode of the propellane derivatives to CT-DNA. Similarly, several reports have shown that the groove binders do not exhibit a large increase in the melting temperature if compared to the intercalators. For examples: Kumar et al. [45] showed that the cationic styryl dye DSMI that binds DNA in the minor groove did not show any effect on the melting temperature of CT- DNA as T_m

Table 2
DNA binding parameters for complexes 5c, 5d and 5f.

Compounds	Binding constant K_a (M^{-1})[a]	n[b]	ΔT_m[c] (°C)	*Hoechst* DC_{50} (μM)[d]	*DAPI* DC_{50} (μM)[d]
5c	$0.39 \times 10^5 \pm 5291$	25.8 ± 0.12	2.18	9.1 ± 2.5	6.2 ± 1.6
5d	$0.10 \times 10^5 \pm 623.0$	30.8 ± 0.08	1.93	19.1 ± 3.7	17.5 ± 5.1
5f	$0.30 \times 10^5 \pm 8243$	25.9 ± 0.25	1.92	33.7 ± 5.1	15.3 ± 8

[a] DNA binding constant by UV–vis spectroscopy method.
[b] [Polynucleotide Phosphate]/([Bound compound]) Calculated from the UV–Vis titrations of compounds with ds-Polynucleotides.
[c] Change in the melting temperature of CT-DNA.
[d] The concentration of each inhibitor needed to displace 50% DAPI or Hoechst 33258 from the DNA minor groove at saturating binding levels.

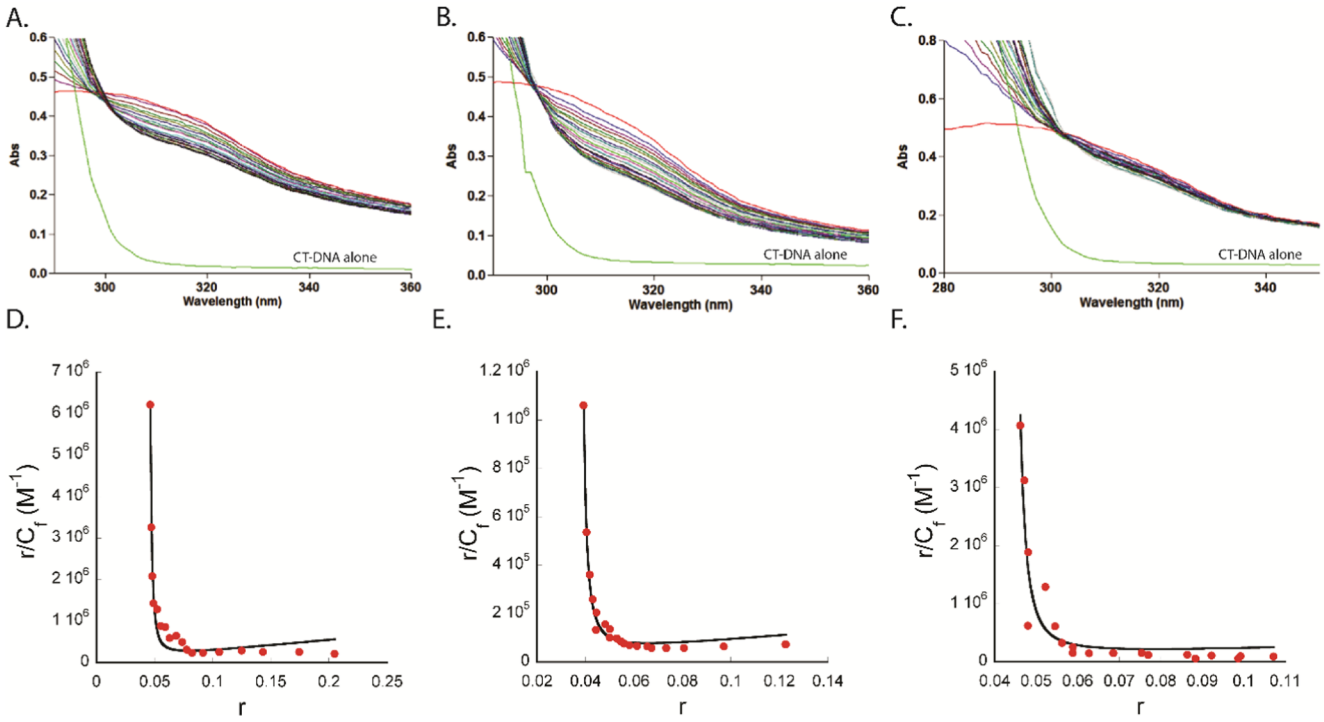

Fig. 3. Changes of UV/vis spectra of 5c (A) at 20 μM, 5d (B) at 20 μM and 5f (C) at 20 μM; upon the titration of CT-DNA at pH = 7, (buffer 50 mM sodium cacodylate containing 1% DMSO). Scatchard plot of 5c (D), 5d (E) and 5f (F)–DNA binding. The absorbance at 315 nm were fitted to Eq. (1) (the methods section).

was estimated to be 80 °C in absence and presence of DSMI. Ma et al. [46] has reported the binding mode of Aflatoxin B1 (AFB1) and aflatoxin G1 (AFG1) to CT-DNA to be mainly through the groove. The binding mode that was evidenced by showing that the AFB1 and AFG1 caused a limited change in CT-DNA melting temperature with ΔT_m of 1 and 2 °C respectively. Sarwar et al. [47] have investigated the binding mode of coumarin to DNA. T_m of CT-DNA in absence and presence of coumarin was 66.8 ± 1 and 68.3 ± 1 respectively, suggesting a limited effect of coumarin on the DNA stability and supported their notion that coumarin possibly binds the minor groove of the Ct-DNA.

2.2.2.3. Viscosity studies. CT-DNA viscosity changes upon interaction with any ligand have been widely used as a marker for the possible binding mode in solution [49,50]. If the interaction is accompanied by an increase in viscosity, this can be evidence of an intercalation mechanism, where the DNA helix lengthens to accommodate ligand binding. A decrease in viscosity results from partial intercalation that only causes bending or possibly shortening of the DNA helix. While, DNA groove binders are reported to cause limited (positive or negative) or no change in viscosity [46,47,49,51]. For example the groove binder Hoechst 33258 does not affect the relative viscosity of CT-DNA solution as it has been reported to have no effect on the axial length of the DNA helix [50,52]. As shown in Fig. 5A, we followed the change in the values of relative specific viscosity $(\eta/\eta 0)^{1/3}$, (where η and $\eta 0$ are the specific viscosity of CT-DNA in the presence of different doses of each propellane derivative or 10% 1,4-dioxane) as a function of r (r = [Ligand]/[CT-DNA], the results emphasized a very limited increase in the viscosity caused by the three derivatives. The ability of the compounds to increase the viscosity of DNA follows the order of **5f** > **5c** > **5d**, where the cyclohexane substituent was the most effective in enhancing viscosity compared to the benzyl or allyl derivatives. Although the propellane derivatives exhibited dose response viscosity enhancement, the increase was limited if compared to the effect of Cisplatin (Fig. 5A), a known DNA intercalator reported to have a pronounced enhancement on CT-DNA viscosity [53]. These observations suggest that the minor effect on viscosity of the propellanes may be a result of binding the DNA groove without having a drastic effect on the axial length of DNA (Fig. 5A).

2.2.2.4. Circular dichroism spectroscopy. Circular dichroism provides a more detailed study of the possible conformational changes that happen to the DNA helix upon interaction with a ligand. In this experiment, we recorded the CD spectra of 50 μM calf thymus DNA in the absence and presence of 20 μM of each propellane derivative. As expected, the CT-DNA (Fig. 5B) showed two bands in the UV region, one at 245 nm (negative band) caused by the right-handed helicity and one at 275 nm (positive band) due to base stacking [48,50]. The interaction of CT-DNA with the three derivatives resulted in small increase in the intensity of the positive band of free CT-DNA while **5d** is the only derivative that caused a limited change in the negative band (Fig. 5B). Suggesting different effects of the derivatives with benzyl and cyclohexyl substituents (**5c** and **5f**) if compared to the allyl derivative (**5d**). Several reports have shown that the non-intercalative DNA binding results in limited to no change in the DNA CD spectra if compared to the DNA intercalators. The groove binding and electrostatic interaction have minor perturbation on the base stacking and helicity bands making them less efficient in changing the DNA helix conformation [46,47,54]. Although, a recent study highlights the limitation of the CD technique in identifying the mode of ligand binding to DNA [55]. The limited changes of the CD spectra that were observed by the propellane derivatives (Fig. 5B) still suggest a non-intercalative binding mode rather than an intercalative one that is expected to cause a more drastic effect on the recorded Cd spectra.

2.2.2.5. Dye displacement assays. These assays were performed to investigate the possible binding mode of the propellanes to the DNA helix. The DNA binding mode can be examined using a DNA binding dye that has a known, well-characterized, binding mode. Replacing such a dye by a ligand may suggest the ligand binding site. Thus, intercalator ligands are expected to replace an intercalator dye, such as ethidium bromide (EB) or thiazole orange (TO), while a groove binder is expected to replace a groove binding dye, such as DAPI or Hoechst

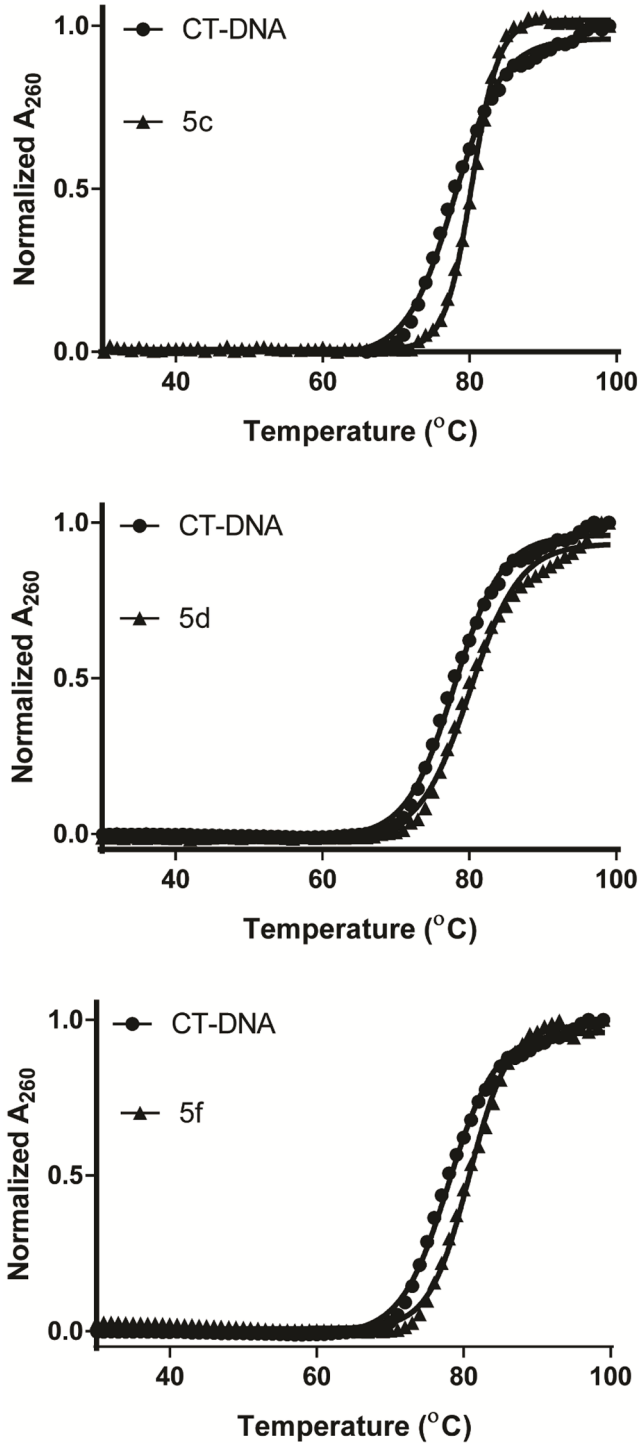

Fig. 4. Plots of the Melting curves of ct-DNA (100 μM) in absence and presence of 50 uM of 1, 2 and 3 at pH = 7.0 (buffer 50 mM Na-cacodylate containing 1% 1,4-Dioxane). Experiments have been repeated two times and the data were consistent.

33258 [46,47,52,56,57]. In this experiment, we tested the effect of the new propellane derivatives on the ability of EB or TO dye to intercalate with CT-DNA and DAPI or Hoechst 33258 dye to bind the CT-DNA groove. DAPI has been reported to bind the DNA minor groove (in the case of A–T rich DNA) in addition to its ability to intercalate with the DNA (in the case of G–C rich DNA) [56,58]. The calf thymus DNA used in this study is 41.9 mol % G-C and 58.1 mol % A-T, which makes DAPI to act mostly as a minor groove binder in this experiment. Hoechst

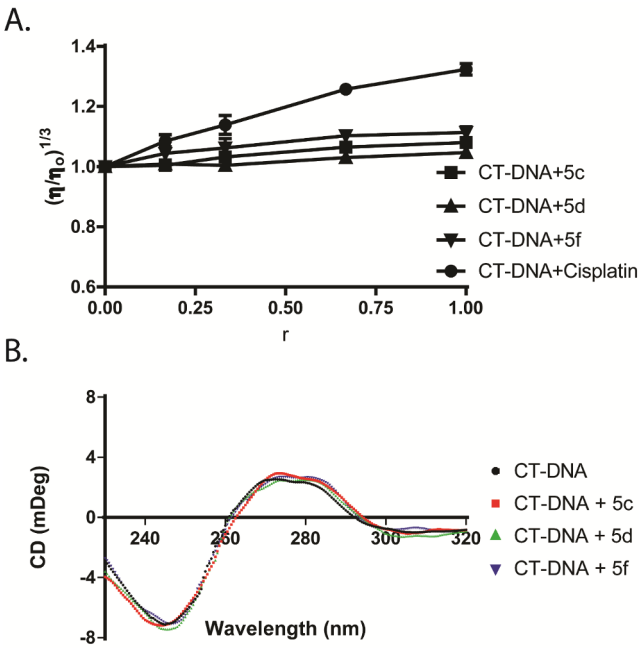

Fig. 5. (A) Dose response effect of 5c, 5d, 5f and Cisplatin on the relative viscosity of CT-DNA at room temperature, [CT-DNA] = 300 μM. Three independent experiments were performed and average values are shown, the error bars represent ± SD. (B) Circular dichroism spectra of CT-DNA (50 μM) in the absence and presence of 5c, 5d and 5f (20 μM) at pH = 7, (buffer 50 mM sodium cacodylate containing 0.4% 1,4-Dioxane). The cuvette path length was 10 mm. Two independent experiments were performed and average values were calculated.

33258 dye is another well-known groove-binder [42]. The binding stoichiometry of DAPI and Hoechst 3328 with CT-DNA has been reported to be 20 base pairs for each dye molecule and the dissociation constants were estimated to be 5 and 3 nM respectively [52]. Ethidium bromide and thiazole orange were reported to have binding stoichiometry of 1.5 base pairs for each dye molecule which is consistent among all DNA intercalators. Their dissociation constants were estimated to be 0.14 and 0.5 μM respectively [52,59].

Using 40 μM CT-DNA, we examined the ability of the new propellanes to displace these dyes at a saturating binding level (2 μM TO, EB or Hoechst 33258 and 6 μM DAPI). The addition of EB or TO to CT-DNA exhibited a drastic fluorescence enhancement due to their intercalation within the DNA base pairs. The continuous addition of different doses of each propellane did not show any significant change in the fluorescence intensity (Fig. 6C and 6D). Suggesting the inability of these propellanes to replace either EB or TO from DNA helix and provide another evidence for the non-intercalative binding mode [46,47]. In the same time and as shown in Fig. 6A and 6B, the three propellane derivatives **5c**, **5d** and **5f** were able to replace the minor groove binder Hoechst 33258 dye from CT-DNA in a dose dependent manner with EC_{50}′s 9, 19 and 34 μM respectively (Table 2) as well as the DAPI dye with EC_{50}′s of 6.2, 17.5 and 15.3 μM respectively (Table 2). Several previous reports have shown groove binding molecules replacing Hoechst 33258 [46,47] or DAPI [56–58] dye from the minor groove of the DNA helix, resulting in decreased fluorescence intensity of Hoechst-DNA or DAPI-DNA system. These experiments suggest the binding mode of these new propellanes to be groove binding rather than intercalation, the observation that requires several future experiments to be confirmed.

2.2.3. Anticancer activity

The results mentioned above support our hypothesis that propellane derivatives designed to carry planar polycyclic ligands can interact with

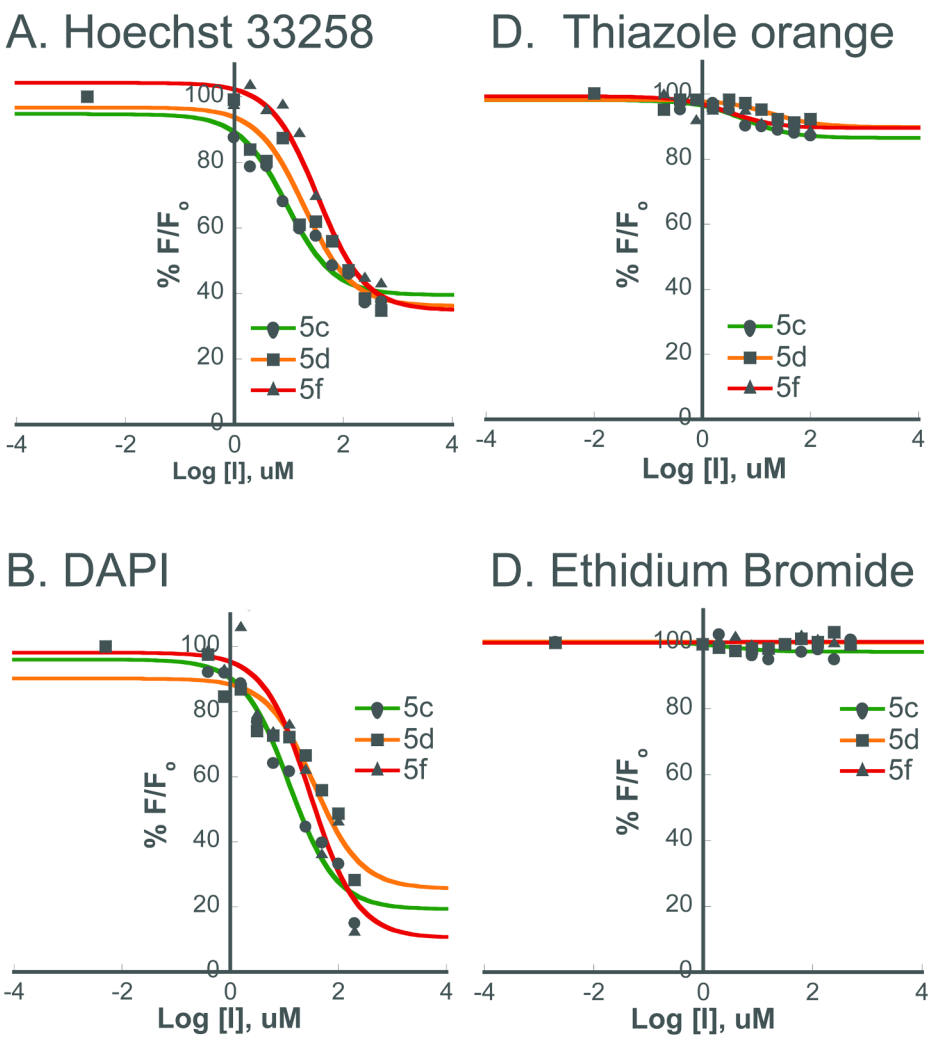

Fig. 6. (A) % Relative fluorescence intensity of titration of CT-DNA (40 μM) and Hoechest 33258 (2 μM) (B) CT-DNA (40 μM) and DAPI (6 μM) (C) CT-DNA (40 μM) and Thiazole Orange (2 μM) (D) CT-DNA (40 μM) and Ethidium Bromide (2 μM) with different doses of each inhibitor. Values represent the normalized average of the fluorescence intensity recorded for three different wells per each inhibitor concentration.

DNA and we provide data supporting the notion that they act as non-intercalative binders probably through the DNA groove. It was therefore important to study the molecular mechanisms underlying the anti-proliferative effects of these compounds in a cancer cell model, such as the non-small cell lung cancer cell line A549.

2.2.3.1. Propellane derivatives induce DNA damage and inhibit the growth of non-small cell lung cancer cell line A549. Induction of DNA damage is one of the major drivers of cancer cell growth arrest and death. Several generations of antineoplastic agents work mainly by induction of DNA damage [60]. Numerous reports have shown that some DNA minor groove binders can cause DNA damage even without acting as DNA alkylating agents. For example, Varadarajan et al. have emphasized the DNA damage and cytotoxicity caused by the minor groove binding of several methyl sulfonate esters [60], while Bales et al. have studied the mechanism of DNA damage caused by the minor groove binding of copper-phenanthroline conjugates in several cancer cell lines [61].

S009-131, a coumarin-chalcone hybrid, has been reported to exhibit anti-proliferative and anti-tumour activity. Its ability to induce DNA damage resulted from its potential binding to the DNA minor groove. Incubation of cancer cells with S009-131 resulted in an enhanced γH2AX phosphorylation level (a well-known DNA damage marker) where highest expression was observed at 24 h [62]. And finally Saini et al. have introduced a small molecule named CT-1, as an orally active minor groove binder, it induces DNA damage in several breast cancer cell lines, leading to p53-dependent apoptosis and cell death [63].

To examine the effect of the newly developed groove binders on DNA damage in A549 cells, we treated the cells with different doses of each inhibitor for 12 hrs and then the effect of the inhibitors on γ-H2AX phosphorylation at Ser139 was monitored by immunoblotting. As mentioned earlier, γH2AX is a DNA damage response signaling protein, whose phosphorylation is an important marker for DNA damage. As shown in Fig. 7A, 5c, 5d and 5f induced γH2AX phosphorylation in a dose dependent manner, with robust induction at 25 μM although 10 μM of **5f** was enough to induce the DNA damage. Interestingly, as shown previously with other groove binders, the DNA damage caused by the propellane derivatives was accompanied by cellular growth arrest. Fig. 7B shows a dose-response suppression of A549 cell proliferation by **5c**, **5d** and **5f** with IC_{50}s of 2.2, 5.2 and 2.6 μM after 72 h of treatment. The effect of cisplatin, a standard DNA intercalator, on A549 cell proliferation was examined in the same experiment (Fig. 7B) and showed IC_{50}s of 10 μM. The lower IC_{50} observed for compound **5c** and **5f** was mainly explained by their ability to induce the DNA damage at considerably lower dose than **5d** as assessed after 12 h of treatment and shown in Fig. 6A besides their enhanced affinity towards DNA helix that were estimated in Table 2. The enhanced hydrophobicity of **5c** and **5f** may also improve their cellular internalization if compared to **5d**.

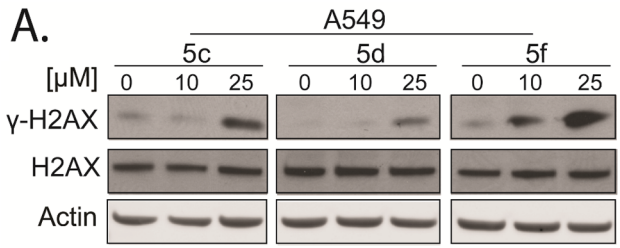

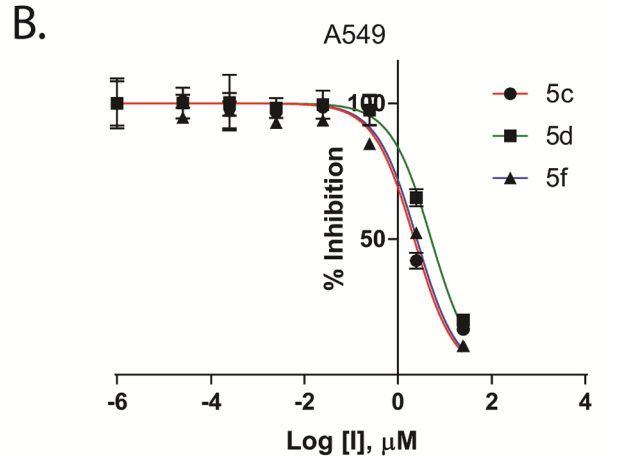

Inhibitory activity on A549 Cell growth	
Comp	IC50 (μM) after 72 Hrs
5c	2.24±1.1
5d	5.20±1.0
5f	2.60±1.2
Cisplatin	10.2±2.0

Fig. 7. The DNA binding properties of 5c, 5d and 5f induced the DNA damage and inhibited the proliferation of the Non-Small Cell Lung Cancer A549 cell line. (A) Whole-cell extracts of A549 cells treated with different doses of 5c, 5d and 5f for 12 hrs, were immunoblotted for phosphorylated DNA damage response signaling protein γH2AX (pH2AX-Ser139). Pan-actin was used as a loading control. (B) The anti-proliferative potency of 5c, 5d, 5f and Cisplatin, A549 cells were incubated with different doses of each compound for 72 h and assessed the resultant impact on cell viability by the MTS assay (Promega) (Error bars: ± Standard Deviation (n = 3)) from which half-inhibitory (IC_{50} ± SEM) concentrations were derived and shown in the down table.

2.2.3.2. Apoptosis induction in non-small cell lung cancer cell line A549. As a consequence of the DNA damage induction, apoptosis is known to be the potential route of cell death [64]. Hoechst 33258, a minor groove binding dye, has been reported to act as a potent inducer of apoptosis in several human mesothelioma cell lines [65]. Saini et al. introduced a curcumin-triazole conjugate as another example of a minor groove binder that inhibited the viability of breast cancer cell lines by causing cell cycle arrest at the S phase and induction of apoptosis [63]. Numerous benzimidazole derivatives have also been reported as minor groove binders, and for instance, 5-Phenyl-2-*p*-tolyl-1*H*-benzimidazole has been shown to induce the intrinsic pathway of apoptosis in leukemia cell lines by activating caspase 9 and caspase 3 [66].

After justifying the ability of the new propellane derivatives as DNA damage inducers, we also examined their ability to trigger apoptosis. Four doses of each derivative were tested in A549 cells (0, 10, 100 and 200 μM of **5c**, **5d** and **5f**). Fig. 8A represents the percentage of the cells that showed early and late apoptosis after 40 and 60 hrs of treatment. It is clear that the three propellane derivatives induce the apoptosis of A549 cells in a dose-dependent manner, as judged by single cell assays using Annexin V and Caspase 3/7 activity as markers (visualized using the IncuCyte zoom microscope). Moreover, treatment of A549 cells with different doses of **5c**, **5d** and **5f** resulted in an increase in cleaved PARP, another marker of apoptosis induction [67]. These data support the notion that the induction of DNA damage and apoptosis can be the major mechanisms of death caused by the new propellane derivatives.

3. Conclusion

It has been reported that numerous natural products containing the propellane substructure exhibit cytotoxicity against several cancers. The aim of this study was to test the hypothesis that propellane scaffold carrying one or two planar ligands can exhibit cytotoxicity by direct interaction with the DNA helix. We started by designing several furoimidazo[3.3.3]propellanes derivatives (**5a–g**) and developed a new method allowing general and effective synthesis of these derivatives with fairly high yields in a relatively short reaction time with easy work-up procedures. It was found that solvent, temperatures and catalyst may all play a critical role on the reaction efficiency. Also, the electrophilic C/C double bond in the acceptor plays an important role on the type of nucleophilic site of addition. Interestingly, the anti-proliferative activity observed by these compounds against A549 NSCLC cells is directly correlated to their ability to bind CT-DNA (determined using UV–Vis spectroscopy). The ability of the compounds to replace the minor groove binding dyes Hoechst 33258 and DAPI, without any effect on the intercalator dyes ethidium bromide and thiazole orange suggests that these new derivatives may act as groove binders rather than DNA intercalators. This conclusion was supported by UV–Vis spectroscopic data, as well as thermal denaturation, viscosity and CD studies that suggested a non-intercalative binding mode. Finally, the mechanism of cell death caused by these compounds was attributed to their DNA damaging ability and subsequent induction of apoptosis. In this study, we provide a new group of propellane-dependent that probably act as DNA groove binders. Although several future studies are required to support this finding, these new derivatives may act as excellent starting points to develop new drugs that can efficiently bind DNA and cause cancer cell death. In addition, this is the first study that showed a possible mechanism for the cytotoxicity caused by propellane containing compounds, through their ability to interact with DNA in cancer cells.

4. Material and methods

4.1. Chemistry

Melting points (mp's) were recorded on a Gallenkamp melting point apparatus (Gallenkamp, UK), by using open capillaries and are uncorrected. NMR data was recorded on a Bruker AM 400 spectrophotometer (Germany), The ^{1}H NMR (400.13 MHz) and ^{13}C NMR (100.6 MHz). Chemical shifts were reported in ppm from tetramethylsilane using solvent resonance in $CDCl_3$ or DMSO-d_6 solutions as the internal standard. The ^{13}C NMR signals were assigned on the basis of DEPT 135/90 spectra. The mass spectra were obtained on Finnigan MAT 312) (Germany) instrument using electron impact ionization (70 eV). The IR spectra were recorded on Bruker Alpha FT-IR instrument (Germany) with samples prepared as potassium bromide pellets. Thin-layer chromatography (TLC) was performed on precoated plates (silica gel 60 Pf_{254}), and zones were visualized with ultraviolet (UV) light. Elemental analyses were determined by the using an Elemenatar 306 (Germany).

4.1.1. Starting materials

Substituted alkenylidene-hydrazinecarbothioamides **2a–g** were prepared by the reaction of 4-substituted thiosemicarbazide with the proper aldehyde according to the published procedures in literature (**2a**

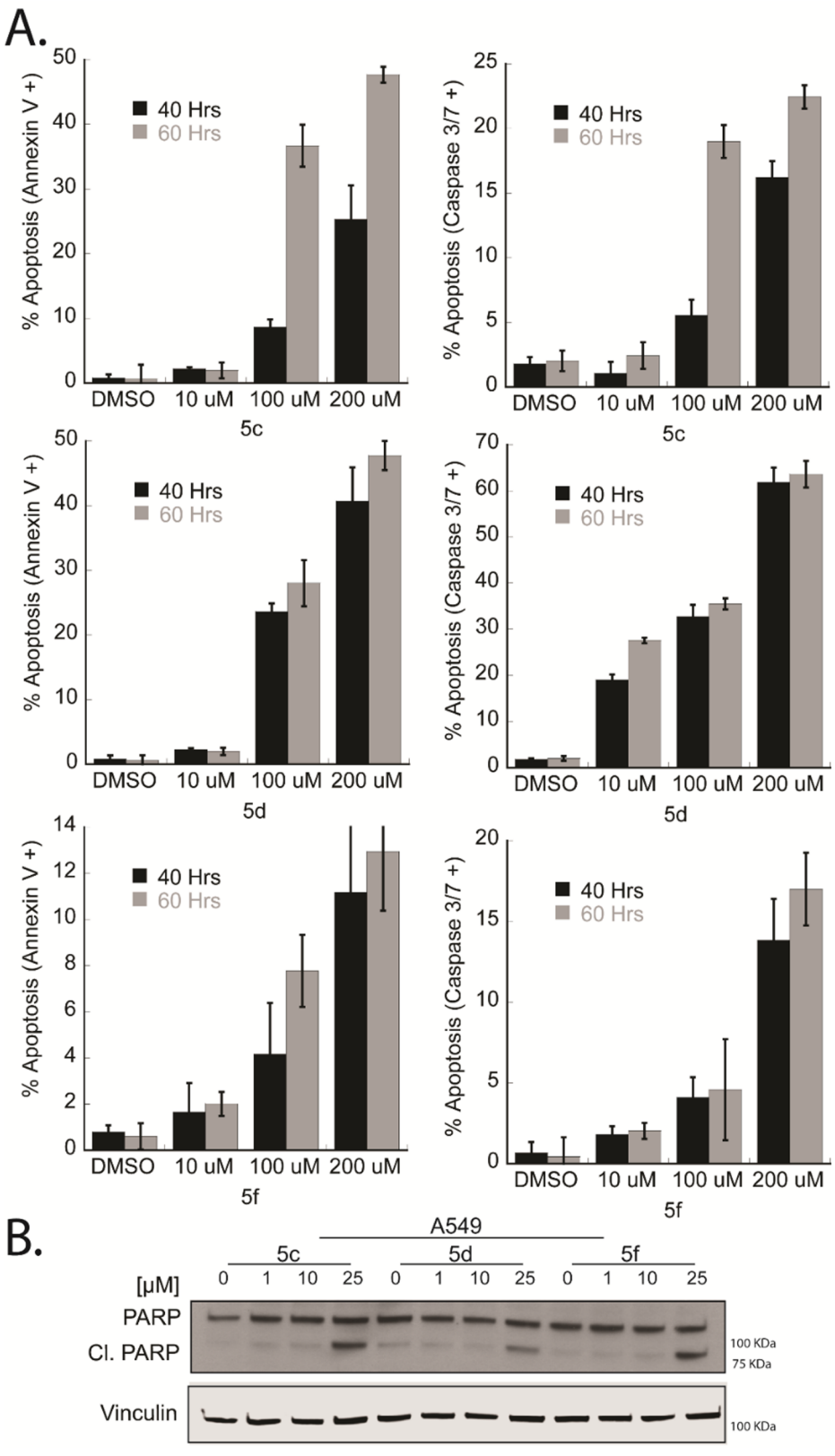

Fig. 8. Treatment of 5c, 5d and 5f induced apoptosis in A549 cell line. (A) Caspase-3/7 activity and Annexin V integration was significantly increased in the treated cells in a dose-dependent manner. The apoptosis analysis was performed using the IncuCyte® ZOOM equipment with a 10X objective at indicated time points. A549 cells were treated with different doses of each compound and the IncuCyte Caspase-3/7 or Annexin V reagents. Apoptotic cells number was normalized to the percentage area coverage (confluency) at the final time point. Error bars: SEM (n = 3). (B) Western blotting of lysates from A549 cells treated for 24 h with 5c, 5d and 5f, immunoblotted for increased level of the apoptosis marker cleaved PARP. Vinculin was used as a loading control.

[68], **2b** [69], **2c** [70], **2d** [68] and **2e** [70]).

(*E*)-*N*-cyclohexyl-2-((*E*)-hex-2-en-1-ylidene)hydrazinecarbothioamide (2f)

Yield: 2.35 g (93%); colorless crystals (EtOH); mp 56–57 °C.

IR (KBr): 3375–3446 (NH), 2928–2852 (Ali-CH), 1643 (C═N), 1517 (NH def. and C−N str.), 1364, 982 (C═S and C−N str.) cm^{-1}.

^{1}H NMR (400 MHz, $CDCl_3$): δ = 0.90–0.94 (t, J = 7.63 Hz, 3H, CH_3), 1.26–1.28 (m, 2H, CH_2), 1.45–1.48 (m, 2H, cyclic-CH_2), 1.62–1.64 (m, 4H, cyclic-CH_2), 1.78–1.80 (m, 4H, cyclic-CH_2), 2.14–2.18 (m, 2H, CH_2), 2.21–2.24 (m, 1H, cyclic-CH), 6.12–6.14 (m, 2H, CH═CH), 7.32 (br, 1H, cyclohexyl-NH), 7.51–7.53 (m, 1H, CH═N), 9.74 (br, 1H, NH).

^{13}C NMR (100 MHz, $CDCl_3$): δ = 13.14 (CH_3), 22.11 (CH_2), 25.16 (CH_2), 26.08 (cyclic-CH_2), 33.42 (cyclic-CH_2), 35.17 (cyclic-CH_2), 41.22 (cyclic-CH), 124.86, 126.23 (CH═CH), 144.16 (CH═N), 176.12 (C═S).

MS: *m/z* (%) = 253 [M^+, 23], 219 (7), 141 (6), 98 (1 0 0), 83 (33), 69 (17).

Anal. Calcd for $C_{13}H_{23}N_3S$ (253.16): C, 61.62, H, 9.15; N, 16.58; S, 12.65. Found: C, 61.73; H, 9.27; N, 16.46; S, 12.55.

(*E*)-*N*-benzyl-2-pentylidenehydrazinecarbothioamide (2g)

Yield: 1.99 g (80%); colorless crystals (EtOH); mp 42–43 °C.

IR (KBr): 3362–3352 (NH), 3062 (Ar−CH), 2953–2864 (Ali-CH), 1632 (C═N), 1603 (Ar−C═C), 1519 (NH def. and C−N str.), 1355, 973 (C═S and C−N) cm^{-1}.

^{1}H NMR (400 MHz, $CDCl_3$): δ = 0.88–0.90 (t, *J* = 7.60 Hz, 3H, CH_3), 1.28–1.32 (m, 2H, CH_2), 1.38–1.42 (m, 2H, CH_2), 2.18–2.22 (m, 2H, CH_2), 4.93 (s, 2H, CH_2Ph), 7.30–7.35 (m, 3H, Ar−H), 7.36–7.41 (m, 3H, Ar−H and CH═N), 7.58 (br, 1H, NH−CH_2Ph), 9.85 (br, 1H, NH).

^{13}C NMR (100 MHz, $CDCl_3$): δ = 13.41 (CH_3), 21.52 (CH_2), 28.12 (CH_2), 33.11 (CH_2), 48.22 (CH_2Ph), 125.64, 127.12, 128.66 (Ar−CH), 137.16 (Ar−C), 148.22 (CH═N), 178.33 (C═S).

Anal. Calcd for $C_{13}H_{19}N_3S$ (249.13): C, 62.61, H, 7.68; N, 16.85; S, 12.86. Found: C, 62.50; H, 7.80; N, 16.96; S, 12.74.

*4.1.2. Synthesis of Furo-imidazo[3.3.3]Propellanes (5**a–g**)*

General procedure: A stirred solution of substituted 1.0 mmol of alkenylidene-hydrazinecarbothioamide **2a–g** in dry THF (20 mL) was added to dicyanomethylene-1,3-indanedione (**1**, 1.25 mmol) in dry THF (15 mL). The mixture was stirred for 3 hrs. The reddish-brown mixture was allowed to stand for 52–72 hrs (monitored by TLC) at room temperature during which time colorless crystals of **5b** were precipitated. The precipitate was filtered off, washed with 5 mL of THF, dried and recrystallized from ethanol. The other derivatives **5a, c–g** were subjected to PLC (plate layer chromatography) using Toluene/ EtOAc (10:7).

(3*aS*,8*bR*)-2-amino-11-((*E*)-((*E*)-hex-2-en-1-ylidene)amino)-4-oxo-9-phenyl-10-thioxo-4*H*-3*a*,8*b*-(epiminomethanoimino)indeno[1,2-*b*]-furan-3-carbonitrile (5a).

Yield: 0.359 g (79%); colorless crystals (EtOH); mp 250–252 °C.

IR (KBr): 3421–3392 (NH_2), 2957–2869 (Ali-CH), 2195 (CN), 1722 (CO), 1649 (C═N), 1577 (Ar−C═C), 1367, 985 (C═S and C−N str.), 1078 (C−O−C) cm^{-1}.

^{1}H NMR (400 MHz, $CDCl_3$): δ_H = 0.82–0.84 (t, 3H, CH_3, *J* = 7.62 Hz,), 1.35–1.37 (m, 2H, CH_2), 2.05–2.11 (m, 2H, CH_2), 6.45–6.48 (m, 2H, CH═CH), 7.44–7.57 (m, 5H, Ar−H and CH═N), 7.78–7.84 (m, 3H, Ar−H), 7.86–7.91 (m, 2H, Ar−H), 8.86–8.88 (br, 2H, NH_2).

^{13}C NMR (100 MHz, DMSO-d_6): δ_C = 14.52 (CH_3), 22.64 (CH_2), 35.87 (CH_2), 47.73 (furan-C3), 82.47 (furan-C4), 103.91 (furan-C5), 111.05, 116.14 (CH═CH), 116.75 (CN), 125.89, 126.71, 126.93, 127.12, 127.64, 128.19, 130.37 (Ar−CH), 136.53, 137.72, 142.93 (Ar−C), 156.41 (CH═N), 169.15 (furan-C-2), 180.17 (C═S), 190.29 (indeno-CO).

MS: *m/z* (%) = 455 ($M^{\cdot+}$, 100), 301 (32), 154 (29), 135 (32).

Anal. Calcd. for $C_{25}H_{21}N_5O_2S$ (455.53): C, 65.92; H, 4.65; N, 15.37; S, 7.04. Found: C, 66.06; H, 4.52; N, 15.22; S, 6.91.

(3aS,8*bR*)-2-amino-11-((*E*)-((*E*)-hex-2-en-1-ylidene)amino)-4-oxo-9-(pyridin-3-yl)-10-thioxo-4*H*-3a,8*b*-(epiminomethanoimino)indeno-[1,2-*b*]furan-3-carbonitrile (5b)

Yield: 0.383 g (84%); colorless crystals (EtOH); mp 244–246 °C.

IR (KBr): 3443–3400 (NH2), 2961–2871 (Ali-CH), 2196 (CN), 1728 (CO), 1648 (CdbndN), 1595 (ArsbndCdbndC), 1371, 987 (CdbndS and CsbndN str.), 1102 (C−O−C) cm^{-1}.

^{1}H NMR (400 MHz, DMSO-d_6): δ_H = 0.92–0.96 (t, 3H, CH_3, *J* = 7.61 Hz,), 1.48–1.54 (m, 2H, CH_2), 2.28–2.31 (m, 2H, CH_2), 6.36–6.39 (m, 2H, CH═CH), 7.60–7.61 (m, 3H, Ar−H and CH═N), 7.75–7.78 (m, 2H, Ar−H), 7.79–7.81 (m, 2H, Ar−H), 7.99–8.02 (m, 1H, Ar−H), 8.50–8.52 (br, 2H, NH_2), 8.71–8.72 (m, 1H, Ar−H).

^{13}C NMR (100 MHz, DMSO-d_6): δ_C = 13.46 (CH_3), 21.24, 34.32 (CH_2), 49.58 (furan-C-3), 81.45 (furan-C-4), 103.86 (furan-C-5), 110.0, 115.7 (CH═CH), 116.64 (CN), 124.25, 124.64, 125.99, 126.94, 132.78, 134.42, 137.09, 140.81(Ar−CH), 139.22, 141.36, 146.39 (Ar−C), 154.06 (CH═N), 168.17 (furan-C-2), 178.93 (C═S), 189.81 (indeno-CO).

MS: *m/z* (%) = 456 ($M^{\cdot+}$, 11), 414 (8), 320 (54), 154 (1 0 0), 136 (72).

Anal. Calcd. for $C_{24}H_{20}N_6O_2S$ (456.52): C, 63.14; H, 4.42; N, 18.41; S, 7.02. Found: C, 62.97; H, 4.51; N, 18.54; S, 6.89.

3*aS*,8*bR*)-2-amino-9-benzyl-11-((*E*)-((*E*)-hex-2-en-1-ylidene)amino)-4-oxo-10-thioxo-4*H*-3*a*,8*b*-(epiminomethanoimino)indeno[1,2-*b*]furan-3-carbonitrile (5c)

Yield: 0.361 g (77%); colorless crystals (EtOH); mp 236–238 °C.

IR (KBr): 3422–3390 (NH_2), 2959–2870 (Ali-CH), 2196 (CN), 1727 (CO), 1647 (C═N), 1603 (Ar−C═C), 1377, 940 (C═S and C−N str.), 1074 (C−O−C) cm^{-1}.

^{1}H NMR (400 MHz, $CDCl_3$): δ_H = 0.87–0.91 (t, 3H, CH_3, *J* = 7.63 Hz,), 1.39–1.41 (m, 2H, CH_2), 2.09–2.11 (m, 2H, CH_2), 5.15 (s, 2H, CH_2Ph), 6.17–6.30 (m, 2H, CH═CH), 7.00–7.19 (m, 3H, Ar−H), 7.55–7.75 (m, 5H, Ar−H and CH═N), 7.80–7.92 (m, 2H, Ar−H), 8.75–8.76 (br, 2H, NH_2).

^{13}C NMR (100 MHz, $CDCl_3$): δ_C = 14.54 (CH_3), 22.45 (CH_2), 35.86 (CH_2), 48.42 (CH_2Ph), 48.77 (furan-C3), 82.03 (furan-C4), 105.53 (furan-C5), 110.7, 116.0 (CH═CH), 116.82 (CN), 125.22, 125.78, 125.87, 127.04, 127.64, 129.35, 132.82 (Ar−CH), 136.61, 137.38, 144.58 (Ar−C), 154.65 (CH═N), 169.81 (furan-C2), 181.03 (C═S), 190.01 (indeno-CO).

MS: *m/z* (%) = 469 ($M^{\cdot+}$, 100), 427 (91, 320 (36), 149 (64), 91 (81), 77 (55).

Anal. Calcd. for $C_{26}H_{23}N_5O_2S$ (469.56): C, 66.50; H, 4.94; N, 14.91; S, 6.83. Found: C, 66.62; H, 5.06; N, 15.10; S, 6.71.

(3*aS*,8*bR*)-9-allyl-2-amino-11-((*E*)-((*E*)-hex-2-en-1-ylidene)amino)-4-oxo-10-thioxo-4*H*-3*a*,8*b*-(epiminomethanoimino)indeno[1,2-*b*]furan-3-carbonitrile (5d)

Yield: 0.306 g (73%); colorless crystals (EtOH); mp 190–191 °C.

IR (KBr): 3403–3332 (NH_2), 2960–2870 (Ali-CH), 2198 (CN), 1720 (CO), 1649 (C═N), 1604 (Ar−C═C), 1373, 935 (C═S and C−N str.), 1092 (C−O−C) cm^{-1}.

^{1}H NMR (400 MHz, $CDCl_3$): δ_H = 0.82–0.85 (t, 3H, CH_3, *J* = 7.63 Hz,), 1.37–1.39 (m, 2H, CH_2), 2.09–2.12 (m, 2H, CH_2), 4.28–4.32 (m, 2H, allyl-CH_2N), 5.04–5.08 (m, 2H, allyl-CH_2 =), 5.77–5.79 (m, 1H, allyl-CH =), 6.06–6.16 (m, 2H, CH═CH), 7.57–7.61 (m, 3H, Ar−H and CH═N), 7.73–7.75 (m, 1H, Ar−H),7.84–7.86 (m, 1H, Ar−H), 8.20–8.23 (br, 2H, NH_2)

^{13}C NMR (100 MHz, $CDCl_3$): δ_C = 14.54 (CH_3), 22.72 (CH_2), 35.85 (CH_2), 47.75 (allyl-CH_2N), 47.72 (furan-C3), 79.66 (furan-C4), 104.0 (furan-C5), 111.12, 116.31 (CH═CH), 116.91 (CN), 118.41 (allyl-CH_2 =), 125.99, 127.02, 128.79, 132.85 (Ar−CH), 134.82 (allyl-CH =), 137.02, 144.86 (Ar−C), 155.05 (CH═N), 169.50 (furan-C2), 181.12 (C═S), 190.70 (indeno-CO).

MS: *m/z* (%) = 419 ($M^{\cdot+}$, 100), 377 (71), 320 (12), 265 (12), 154 (43), 99 (11).

Anal. Calcd. for $C_{22}H_{21}N_5O_2S$ (419.50): C, 62.99; H, 5.05; N, 16.69; S, 7.64. Found: C, 63.16; H, 4.91; N, 16.54; S, 7.72.

(3*aS*,8*bR*)-2-amino-9-ethyl-11-((*E*)-((*E*)-hex-2-en-1-ylidene)amino)-4-oxo-10-thioxo-4*H*-3*a*,8*b*-(epiminomethanoimino)indeno[1,2-*b*]furan-3-carbonitrile (5e)

Yield: 0.289 g (71%); colorless crystals (EtOH); mp 200–202 °C.

IR (KBr): 3409–3321 (NH_2), 2961–2870 (Ali-CH), 2199 (CN), 1721 (CO), 1647 (C═N), 1603 (Ar−C═C), 1376, 934 (C═S and C−N str.), 1084 (C−O−C) cm^{-1}.

^{1}H NMR (400 MHz, DMSO-d_6): δ_H = 0.85–0.88 (t, 3H, CH_3, *J* = 7.65 Hz,), 1.13–1.17 (t, 3H, CH_3, *J* = 6.71 Hz,), 1.40–1.45 (m, 2H, CH_2), 2.14–2.19 (m, 2H, CH_2), 3.83–3.87 (q, 2H, CH_2, *J* = 6.71 Hz,),

6.18–6.30 (m, 2H, CH═CH), 7.82–7.85 (m, 3H, Ar—H and CH═N), 7.94–7.97 (m, 2H, Ar—H), 8.21–8.24 (br, 2H, NH_2).

^{13}C NMR (100 MHz, DMSO-d_6): δc = 13.21 (CH_3), 13.48 (CH_3), 21.32 (CH_2), 34.23 (CH_2), 44.16 (CH_2), 48.02 (furan-C-3), 78.00 (furan-C-4), 104.39 (furan-C-5), 112.0, 115.91 (CH═CH), 116.12 (CN), 125.17, 125.60, 127.58, 128.32 (Ar—CH), 137.28, 144.51 (Ar—C), 157.02 (CH═N), 165.83 (furan-C-2), 179.76 (C═S), 191.08 (indeno-CO).

MS: *m/z* (%) = 407 ($M^{\cdot+}$, 100), 320 (44), 253 (26), 154 (63), 87 (24).

Anal. Calcd. for $C_{21}H_{21}N_5O_2S$ (407.49): C, 61.90; H, 5.19; N, 17.19; S, 7.87. Found: C, 62.02; H, 5.23; N, 17.11; S, 7.93.

(3*aS*,8*bR*)-2-amino-9-cyclohexyl-11-((*E*)-((*E*)-hex-2-en-1-ylidene) amino)-4-oxo-10-thioxo-4*H*-3*a*,8*b*-(epiminomethanoimino)indeno[1,2-*b*]-furan-3-carbonitrile (5f)

Yield: 0.341 g (74%); colorless crystals (EtOH); mp 205–207 °C.

IR (KBr): 3416–3328 (NH_2), 2931–2856 (Ali-CH), 2196 (CN), 1725 (CO), 1650 (C═N), 1601 (Ar—C═C), 1347, 981 (C═S and C—N str.), 1101 (C—O—C) cm^{-1}.

^{1}H NMR (400 MHz, $CDCl_3$): δ_H = 0.84–0.86 (t, 3H, CH_3, *J* = 7.66 Hz,), 1.29–1.39 (m, 4H, cyclohexyl-CH_2), 1.41–1.42 (m, 2H, CH_2), 1.65–1.70 (m, 4H, cyclohexyl-CH_2), 1.80–1.83 (m, 2H, cyclohexyl-CH_2), 2.07–2.11 (m, 2H, CH_2), 2.15–2.17 (m, 1H, cyclohexyl-CH), 6.16–6.18 (m, 2H, CH═CH), 7.58–7.66 (m, 3H, Ar—H and CH═N), 7.77–7.89 (m, 2H, Ar—H), 8.70–8.73 (br, 2H, NH_2).

^{13}C NMR (100 MHz, DMSO-d_6): δc = 14.52 (CH_3), 22.80 (CH_2), 27.24, 30.17, 35.83 (cyclohexyl-CH_2), 35.97 (CH_2), 48.11 (furan-C-3), 59.62 (cyclohexyl-CH), 80.50 (furan-C-4), 104.12 (furan-C-5), 111.64, 116,41 (CH═CH) 116.89 (CN), 124.52, 127.16, 128.99, 132.73 (Ar—CH), 137.33, 145.99 (Ar—C), 154.97 (CH═N), 168.79 (furan-C-2), 181.59 (C═S), 190.37 (indeno-CO).

MS: *m/z* (%) = 461 ($M^{\cdot+}$, 100), 320 (44), 32 (9), 419 (18), 392 (22), 154 (81).

Anal. Calcd. for $C_{25}H_{27}N_5O_2S$ (461.58): C, 65.05; H, 5.90; N, 15.17; S, 6.95. Found: C, 64.91; H, 5.76; N, 15.32; S, 7.07.

(3*aS*,8*bR*)-2-amino-9-benzyl-4-oxo-11-((*E*)-pentylideneamino)-10-thioxo-4*H*-3*a*,8*b*-(epiminomethanoimino)indeno[1,2-*b*]furan-3-carbonitrile (5 g)

Yield: 0.347 g (76%); colorless crystals (EtOH); mp 210–212 °C.

IR (KBr): 3426–3339 (NH_2), 2956–2866 (Ali-CH), 2194 (CN), 1725 (CO), 1651 (C═N), 1580 (Ar—C═C), 1353, 991 (C═S and C—N str.), 1076 (C—O—C) cm^{-1}.

^{1}H NMR (400 MHz, DMSO-d_6): δ_H = 0.93–0.96 (t, 3H, CH_3, *J* = 7.61 Hz,), 1.44–1.46 (m, 2H, CH_2), 1.60–1.62 (m, 2H, CH_2), 2.42–2.44 (m, 2H, CH_2), 5.20 (s, 2H, CH_2Ph), 7.09–7.21 (m, 3H, Ar—H), 7.75–7.83 (m, 5H, Ar—H and CH═N), 7.91–7.96 (m, 2H, Ar—H), 8.30–8.35 (br, 2H, NH_2).

^{13}C NMR (100 MHz, DMSO-d_6): δ_c = 13.45 (CH_3), 21.72 (CH_2), 27.35 (CH_2), 32.03 (CH_2), 47.83 (CH_2Ph), 49.21 (furan-C-3), 80.70 (furan-C-4), 104.87 (furan-C-5), 116.93 (CN), 125.34, 126.04, 127.10, 128.06, 132.65, 133.34, 135.66 (Ar—CH), 136.34, 137.28, 141.29 (Ar—C), 157.22 (CH═N), 167.52 (furan-C-2), 180.05 (C═S), 189.96 (indeno-CO).

MS: *m/z* (%) = 457 ($M^{\cdot+}$, 69), 308 (23), 153 (100).

Anal. Calcd. for $C_{25}H_{23}N_5O_2S$ (457.55): C, 65.63; H, 5.07; N, 15.31; S, 7.01. Found: C, 65.78; H, 4.91; N, 15.19; S, 6.94.

4.1.3. Single crystal X-ray structure determination of 5b

The single-crystal X-ray diffraction study was carried out on a Bruker D8 Venture diffractometer with Photon100 detector at 123(2) K using Cu-Kα radiation (λ = 1.54178 Å. Direct Methods (SHELXS-97) [71] were used for structure solution and refinement was carried out using SHELXL-2014 (full-matrix least-squares on F^2) [72]. Hydrogen atoms were refined using a riding model (H(N) free,). A semi-empirical absorption correction was applied. The hex-2-en-1-ylidene substituent is disordered.

Compound 5b: $C_{24}H_{20}N_6O_2S$, Mr = 456.52 g mol^{-1}, colourless blocks, size 0.22 × 0.08 × 0.04 mm, triclinic, space group *P*-1, a = 10.3144 (4) Å, b = 10.3654 (4) Å, c = 11.3719 (6) Å, α = 68.809 (2)°, β = 80.169 (2)°, γ = 80.674 (2) °, V = 1110.26 (8) $Å^3$, Z = 2, D_{calcd} = 1.336 Mg m^{-3}, F (0 0 0) = 476, μ = 1.58 mm^{-1}, T = 123 K, 13297 measured reflections ($2\theta_{max}$ = 144.0°), 4312 independent reflections [R_{int} = 0.025], 297 parameters, 115 restraints, R_1 [for 4002 › 2σ (I)] = 0.073, wR^2 (for all data) = 0.211, S = 1.03, largest diff. peak and hole = 1.64 e $Å^{-3}$/−1.07 e $Å^{-3}$.

CCDC 1875475 (**5b**) contains the supplementary crystallographic data for this paper. These data can be obtained free of charge from The Cambridge Crystallographic Data Centre via www.ccdc.cam.ac.uk/data_request/cif.

4.2. Biology

4.2.1. Sixty cancer cell lines screening at the NCI

The methodology of the NCI anticancer screening has been described in detail at (http://www.dtp.nci.nih.gov). Briefly, the anticancer assay was performed at approximately 60 human cancer cell lines panel derived from nine different tumor types, in accordance with the protocol of the Drug Evaluation Branch, National Cancer Institute, Bethesda. The tested anilides were added to the culture at a single concentration (10^{-5} M) and the cultures were incubated for 48 h. End point determinations were made with a protein binding dye, SRB. Results for each tested compound were reported as the percent of tumor growth of the treated cells in comparison with the untreated control cells. The percentage growth was evaluated spectrophotometrically versus controls not treated with test agents.

4.2.2. DNA interaction experiments

DNA preparation - CT-DNA or Deoxyribonucleic acid sodium salt from calf thymus (Type I, fibers) was purchased from Sigma-Aldrich and solubilized in 50 mM sodium cacodylate buffer (pH 7), sonicated for 30 min then kept in an orbital shaker for 24 h (at 4 °C) before filtration through 0.45 μm filter. Final molar concentration was determined by measuring the absorbance of the solution at λ = 260 nm, using ε(CT-DNA) = 6600 $mmol^{-1}$ cm^{-2}.

Absorption spectral studies- The UV/vis spectra were obtained on Varian Cary 50 Bio spectrometer using quartz cuvettes (1 cm). The experiments were performed by titrating a fixed concentration of each compound (20 μM) with different concentrations of CT-DNA. The reaction was performed in 50 mM sodium cacodylate buffer (pH 7) containing 1% DMSO. The spectral changes upon continuous DNA titration were recorded and employed to calculate the binding constant (K_a) of each tested compound using both the Scatchard equation and the neighbor exclusion model (Eq (1)) [42,43], where C_f is the concentration of the free compound (probe), *r* is the ratio of the concentration of bound drug C_b to the total binding sites [DNA] and *n* is the binding density. All data were treated using KalediaGraph software.

$$\frac{r}{C_f} = K_a(1 - nr)\left[\frac{(1 - nr)}{[1 - (n - r)r]}\right]^{n-r} \quad (1)$$

The Thermal Denaturation Studies - Thermal melting studies of CT-DNA were performed by following the absorption change at 260 nm as a function of temperature change using Cary 4000 UV–Vis. The Absorbance was recorded over a temperature range of 30–90 °C with a ramp rate of 0.5 °C min^{-1} in 50 mM sodium cacodylate buffer (pH 7) containing 1% 1,4-Dioxane. The melting temperature (Tm) was determined from the derivative plot (dA260/dT vs T) of the melting plot. ΔTm Values were calculated by subtracting Tm of the free CT-DNA from the Tm of the CT-DNA-Drug complex.

Viscosity Studies - The viscosity of 300 μM of the CT-DNA at pH = 7, (buffer 50 mM sodium cacodylate containing 10% 1,4-Dioxane) alone or in combination with different doses of each tested

compounds (50, 100, 200 and 300 μM) were estimated in a final volume of 3 mL using the Ostwald viscometer (at 22 °C). Results were plotted as $(\eta/\eta 0)^{1/3}$ versus the ratio of the concentration of each compound to CT-DNA (r), where η0 is the viscosity of CT-DNA alone while η is the viscosity of CT-DNA in the presence of each tested compound. Viscosity values were estimated from the observed flow time of the solution containing CT-DNA subtracted from the flow time of the used buffer (buffer 50 mM sodium cacodylate containing 10% 1,4-Dioxane) (t0), $\eta = (t - t0)$.

Circular dichroism studies - The possible conformational alteration of CT-DNA due to the interaction with compounds **5c, 5d** and **5f** was investigated using the circular dichroism. The circular dichroism (CD) spectroscopic studies were performed using Jasco J-810 circular dichroism spectropolarimeter at 25 °C. CD spectra of the CT-DNA at a concentration of 50 μM were recorded at pH = 7, (buffer 50 mM sodium cacodylate containing 0.4% 1,4-Dioxane) in absence and presence of 20 μM of each tested compound.

Fluorescence dye displacement assay – The assay was performed using the Victor^3 V Model 1420 plate reader from PerkinElmer (Waltham, MA). Each Dye-DNA complex were formed by mixing 40 μM CT-DNA with 2 μM Ethidium Bromide, 2 μM thiazole orange, 2 μM Hoechst 33258 or 6 μM DAPI in a buffer containing 50 mM sodium cacodylate and 2.5–5% 1,4-Dioxane, (pH 7). Stock solutions of different doses of the tested compounds were prepared in the same buffer and added into the dye-DNA solution. Fluorescence emission was recorded at room temperature with a 1 cm light-path quartz cuvette and 10 nm slit width for both excitation and emission. The EB–DNA mixture was excited at 515 nm, and the emission was recorded at 590 nm. Similarly, excitation wavelengths were 504, 345, and 344 nm for thiazole orange, DAPI and Hoechst 33258, respectively. The emission was recorded at 530 nm for thiazole orange and at 460 nm for DAPI and H33258.

4.2.3. Anticancer activity assays

Cell culture – A549 cell line was cultured in RPMI (Invitrogen) supplemented with 10% (v/v) Fetal Bovine Serum (FBS)-US grade (Invitrogen), 1X Glutamax (Invitrogen), 100 UmL-1 penicillin (Sigma), and 100 gmL-1 streptomycin (Sigma). Cells were cultured in a humidified 5% CO2 incubator at 37 °C. For Western blotting, cells were seeded at 800,000–1000,000 cells per well in a 6-well plate and incubated for 24 hrs before treatment with DMSO or different doses of each compound for 12 or 24 h.

Western Blotting - After drug incubation, cell lysates were prepared in M−PER™ Mammalian Protein Extraction Reagent (ThermoFisher) after washing in PBS (Invitrogen). The lysates were cleared by centrifugation, and Bradford analysis (Bio-Rad) was used to measure the protein concentration. Lysates containing 60 μg of total protein were fractionated on a 10% SDS polyacrylamide gel (Bio-Rad) and transferred to Hybond-P PVDF Membrane (GE Healthcare). Primary antibodies were incubated overnight at 4 °C using 1:1000 antiphospho-H2AX (Ser-139), rabbit mAb (Cell Signaling Technology); 1:1000 anti-H2AX (D17A3) rabbit mAb (Cell Signaling Technology); 1:1000 anti-PARP (46D11) rabbit mAB (Cell Signaling Technology); 1:1000 anti-cleaved-PARP (D214) rabbit polyclonal Abs (Cell Signaling Technology); 1/2000 anti-Vinculin (E1E9V) XP rabbit mAb (Cell Signaling Technology) and 1:5000 antiactin, clone 4 mouse mAb (Millipore). Either anti-rabbit (Bio-Rad) or anti-mouse (Cell Signaling Technology) horseradish peroxidase-conjugated secondary antibodies and Western Bright ECL Western Blotting Reagents (Advansta) were used to develop the blots. All experiments were reproduced in independent experiments. All experiments were performed two times.

Cells proliferation assays - The MTS assay (CellTiter 96® AQueous One Solution Cell Proliferation Assay from Promega) was used to detect the proliferation of cells following the manufacturer protocol. All experiments were performed in triplicate.

IncuCyte apoptosis analysis - In each well of a 96 well plate, A549 cells were seeded (2000 cells/well). Cells were allowed to adhere for 24 h before treatment. Cells were treated with different doses of each compound in the presence of constant concentration of the lncuCyte Caspase-3/7 or Annexin V reagent following the manufacturer's protocol. Cells were incubated and imaged in the lncuCyte® ZOOM microscope with a 10X objective at different time points. The number of apoptotic cells was normalized to the percentage confluency at each time point to account for cell proliferation.

Acknowledgements

We acknowledge the NCI for inclusion of our compounds in their screening program. Funding by The Cancer Prevention and Research Institute of Texas (CPRIT) grant (RP160657), USA; the National Institutes of Health (R01 GM123252), USA and The Welch Foundation (F-1390), USA to KN Dalby is also acknowledged.

Appendix A. Supplementary material

Supplementary data to this article can be found online at https://doi.org/10.1016/j.bioorg.2019.02.027.

References

[1] A.M. Dilmac, E. Spuling, A. de Meijere, S. Bräse, Propellanes-from a chemical curiosity to "explosive" materials and natural products, Angew. Chem. Int. Ed. Engl. 56 (21) (2017) 5684–5718, https://doi.org/10.1002/anie.201603951.
[2] M. Rey-Carrizo, M. Barniol-Xicota, C. Ma, M. Frigole-Vivas, E. Torres, L. Naesens, S. Llabres, J. Juarez-Jimenez, F.J. Luque, W.F. DeGrado, R.A. Lamb, L.H. Pinto, S. Vazquez, Easily accessible polycyclic amines that inhibit the wild-type and amantadine-resistant mutants of the M2 channel of influenza A virus, J. Med. Chem. 57 (13) (2014) 5738–5747, https://doi.org/10.1021/jm5005804.
[3] J. Qian-Cutrone, Q. Gao, S. Huang, S.E. Klohr, J.A. Veitch, Y.-Z. Shu, Arthrinone, A Novel fungal metabolite from Arthrinium sp. FA 1744, J. Natural Prod. 57 (12) (1994) 1656–1660, https://doi.org/10.1021/np50114a006.
[4] A. Rezvanian, A. Alizadeh, Powerful approach to synthesis of fused oxa-aza[3.3.3] propellanes via chemoselective sequential MCR in a single pot, Tetrahedron 68 (49) (2012) 10164–10168, https://doi.org/10.1016/j.tet.2012.09.101.
[5] Y.Z. Tang, Y.H. Liu, J.X. Chen, Pleuromutilin and its derivatives-the lead compounds for novel antibiotics, Mini-Rev. Med. Chem. 12 (1) (2012) 53–61, https://doi.org/10.2174/138955712798868968.
[6] M. Konishi, H. Ohkuma, T. Tsuno, T. Oki, G.D. VanDuyne, J. Clardy, Crystal and molecular structure of dynemicin A: a novel 1,5-diyn-3-ene antitumor antibiotic, J. Am. Chem. Soc. 112 (9) (1990) 3715–3716, https://doi.org/10.1021/ja00165a097.
[7] M. Chu, I. Truumees, M.G. Patel, V.P. Gullo, M.S. Puar, A.T. McPhail, Structure of Sch 49209: a novel antitumor agent from the fungus Nattrassia mangiferae, J. Organic Chem. 59 (5) (1994) 1222–1223, https://doi.org/10.1021/jo00084a052.
[8] X. Tian, L. Li, Y. Hu, H. Zhang, Y. Liu, H. Chen, G. Ding, Z. Zou, Dichrocephones A and B, two cytotoxic sesquiterpenoids with the unique [3.3.3] propellane nucleus skeleton from Dichrocephala benthamii, RSC Adv. 3 (21) (2013) 7880–7883, https://doi.org/10.1039/c3ra23364b.
[9] H. Zhu, C. Chen, Q. Tong, X.N. Li, J. Yang, Y. Xue, Z. Luo, J. Wang, G. Yao, Y. Zhang, Epicochalasines A and B: two bioactive Merocytochalasans Bearing Caged Epicoccine Dimer Units from Aspergillus flavipes, Angew. Chem. Int. Ed. Engl. 55 (10) (2016) 3486–3490, https://doi.org/10.1002/anie.201511315.
[10] G. Zuber, J.C. Quada, S.M. Hecht, Sequence selective cleavage of a DNA Octanucleotide by Chlorinated Bithiazoles and Bleomycins, J. Am. Chem. Soc. 120 (36) (1998) 9368–9369, https://doi.org/10.1021/ja981937r.
[11] C. Bailly, Topoisomerase I poisons and suppressors as anticancer drugs, Curr. Med. Chem. 7 (1) (2000) 39–58, https://doi.org/10.2174/0929867003375489.
[12] O. Seitz, DNA and RNA Binders. From Small Molecules to Drugs. Vols. 1 & 2. Edited by Martine Demeunynck, Christian Bailly and W. David Wilson, Angew. Chem. Int. Ed. 42 (41) (2003), https://doi.org/10.1002/anie.200385976.
[13] S.M. Hecht, Bleomycin: new perspectives on the mechanism of action, J. Nat. Prod. 63 (1) (2000) 158–168, https://doi.org/10.1021/np990549f.
[14] T. Ghosh, B.G. Maiya, A. Samanta, A.D. Shukla, D.A. Jose, D.K. Kumar, A. Das, Mixed-ligand complexes of ruthenium(II) containing new photoactive or electroactive ligands: synthesis, spectral characterization and DNA interactions, J. Biol. Inorg. Chem. 10 (5) (2005) 496–508, https://doi.org/10.1007/s00775-005-0660-6.
[15] F.Q. Liu, Q.X. Wang, K. Jiao, F.F. Jian, G.Y. Liu, R.X. Li, Synthesis, crystal structure, and DNA-binding properties of a new copper (II) complex containing mixed-ligands of 2,2′-bipyridine and p-methylbenzoate, Inorg. Chim. Acta 359 (5) (2006) 1524–1530, https://doi.org/10.1016/j.ica.2005.12.035.
[16] H. Song, J.T. Kaiser, J.K. Barton, Crystal structure of Delta-[Ru(bpy)(2)dppz](2)(+) bound to mismatched DNA reveals side-by-side metalloinsertion and intercalation, Nat. Chem. 4 (8) (2012) 615–620, https://doi.org/10.1038/nchem.1375.
[17] B.M. Zeglis, V.C. Pierre, J.K. Barton, Metallo-intercalators and metallo-insertors, Chem. Commun. (Camb.) 44 (2007) 4565–4579, https://doi.org/10.1039/b710949k.
[18] A. Ali, S. Bhattacharya, DNA binders in clinical trials and chemotherapy, Bioorg.

Med. Chem. 22 (16) (2014) 4506–4521, https://doi.org/10.1016/j.bmc.2014.05.030.
[19] G.M. Blackburn, Royal Society of Chemistry (Great Britain), Nucleic acids in chemistry and biology, third ed., RSC Pub, Cambridge, 2006.
[20] P.L. Hamilton, D.P. Arya, Natural product DNA major groove binders, Nat. Prod. Rep. 29 (2) (2012) 134–143, https://doi.org/10.1039/c1np00054c.
[21] P.G. Baraldi, A. Bovero, F. Fruttarolo, D. Preti, M.A. Tabrizi, M.G. Pavani, R. Romagnoli, DNA minor groove binders as potential antitumor and antimicrobial agents, Med. Res. Rev. 24 (4) (2004) 475–528, https://doi.org/10.1002/med.20000.
[22] A. Alizadeh, F. Bayat, L. Moafi, L.-G. Zhu, 5-Hydroxybenzo[g]indoles formation from oxa-aza[3.3.3]propellanes, Tetrahedron 71 (42) (2015) 8150–8154, https://doi.org/10.1016/j.tet.2015.08.035.
[23] A. Alizadeh, A. Rezvanian, L.G. Zhu, Synthesis of heterocyclic [3.3.3]propellanes via a sequential four-component reaction, J. Org. Chem. 77 (9) (2012) 4385–4390, https://doi.org/10.1021/jo300457m.
[24] A. Alizadeh, A. Rezvanian, L.-G. Zhu, Chemo- and Regioselective 4CR Synthesis of Oxathiaaza[3.3.3]propellanes via Sequential C-S, C–N and C–O Bond Formation in a Single Pot, Synlett 23 (17) (2012) 2526–2530, https://doi.org/10.1055/s-0032-1317181.
[25] I. Yavari, A. Malekafzali, S. Skoulika, Tandem synthesis of trichloromethylated [3.3.3]propellanes from trichloroacetamidines and a ninhydrin–malononitrile adduct, Tetrahedron Lett. 55 (20) (2014) 3154–3156, https://doi.org/10.1016/j.tetlet.2014.03.124.
[26] N. Chen, S. Xia, M. Zou, X. Shao, Bridged heterocyclic neonicotinoid analogues: design, synthesis, and insecticidal activity, Res. Chem. Intermed. 41 (8) (2014) 5293–5300, https://doi.org/10.1007/s11164-014-1631-8.
[27] L.-J. Zhang, C.-G. Yan, One-pot domino reactions for synthesis of heterocyclic [3.3.3]propellanes and spiro[cyclopenta[b]pyridine-4,2′-indenes], Tetrahedron 69 (24) (2013) 4915–4921, https://doi.org/10.1016/j.tet.2013.04.048.
[28] A.A. Hassan, N.K. Mohamed, M.M. Makhlouf, S. Bräse, M. Nieger, Synthesis of Oxa-aza- and Bis-oxathiaaza[3.3.3]propellanes from Dicyanomethylene-1,3-indanedione and 2,5-Dithiobiureas, Synthesis 47 (19) (2015) 3036–3042, https://doi.org/10.1055/s-0034-1380447.
[29] A.A. Hassan, K.M.A. El-Shaieb, A.S. Abd El-Aal, S. Bräse, M. Nieger, Synthesis of bis-oxathiaaza[3.3.3]propellanes via nucleophilic addition of (1, ω-alkanediyl)bis(N′-organylthioureas) on dicyanomethylene-1,3-indanedione, ARKIVOC (Gainesville, FL, U. S.) (5) (2016) 406–415, https://doi.org/10.3998/ark.5550190.p009.715.
[30] A.A. Aly, E.M. El-Sheref, M.E.M. Bakheet, M.A.E. Mourad, S. Bräse, M.A.A. Ibrahim, M. Nieger, B.K. Garvalov, K.N. Dalby, T.S. Kaoud, Design, synthesis and biological evaluation of fused naphthofuro[3,2-c] quinoline-6,7,12-triones and pyrano[3,2-c] quinoline-6,7,8,13-tetraones derivatives as ERK inhibitors with efficacy in BRAF-mutant melanoma, Bioorg. Chem. 82 (2018) 290–305, https://doi.org/10.1016/j.bioorg.2018.10.044.
[31] A.A. Aly, E.M. El-Sheref, M.E.M. Bakheet, M.A.E. Mourad, A.B. Brown, S. Brase, M. Nieger, M.A.A. Ibrahim, Synthesis of novel 1,2-bis-quinolinyl-1,4-naphthoquinones: ERK2 inhibition, cytotoxicity and molecular docking studies, Bioorg. Chem. 81 (2018) 700–712, https://doi.org/10.1016/j.bioorg.2018.09.017.
[32] A.A. Hassan, N.K. Mohamed, L.E. Abd El-Haleem, S. Brase, M. Nieger, Synthesis of New Furo-Imidazo[3.3.3]propellanes, Curr. Org. Synth. 13 (3) (2016) 426–431, https://doi.org/10.2174/1570179412666150513003813.
[33] A.A. Hassan, S.K. Mohamed, F.F. Abdel-Latif, S.M. Mostafa, M. Abdel-Aziz, J. Mague, M. Akkurt, A novel method for the synthesis of Furo-imidazo[3.3.3] propellanes from Thiocarbonohydrazides, Synlett 27 (03) (2015) 412–416, https://doi.org/10.1055/s-0035-1560828.
[34] K. Gewald, R. Schindler, Cyclisierungen mit Cyanthioacetamid in Gegenwart von Schwefel, Journal für Praktische Chemie 332 (2) (1990) 223–228, https://doi.org/10.1002/prac.19903320213.
[35] R. Radeglia, Kalinowski, H.-O.; Berger, St.; Braun, S.:13C-NMR-Spektroskopie. XII, 685S., 142Abb., 200 Tab., Format 15,5 × 23cm. Stuttgart-New York: Georg Thieme Verlag 1984. brosch. 98,-DM, Journal für Praktische Chemie 327(5) (1985) 878–879, https://doi.org/10.1002/prac.19853270523.
[36] A.A. Hassan, H.S. Shehata, D. Döpp, Formation of 5-alkylidenepyrazol-4(1 < I > H < /I >)-ones and 3-amino-6-aryl-5-cyanopyridazine-4-carboxylates from arenealdehyde thiosemicarbazones and unsaturated 1,2-diesters, J. Chem. Res. 2008 (12) (2008) 725–730, https://doi.org/10.3184/030823408x390208.
[37] K. Starcevic, M. Kralj, I. Piantanida, L. Suman, K. Pavelic, G. Karminski-Zamola, Synthesis, photochemical synthesis, DNA binding and antitumor evaluation of novel cyano- and amidino-substituted derivatives of naphtho-furans, naphtho-thiophenes, thieno-benzofurans, benzo-dithiophenes and their acyclic precursors, Eur. J. Med. Chem. 41 (8) (2006) 925–939, https://doi.org/10.1016/j.ejmech.2006.03.012.
[38] Z. Cheng-Yong, X. Xiao-Li, Y. Pin, Studies on DNA binding to metal complexes of Sal2trien, Biochemistry (Mosc) 72 (1) (2007) 37–43.
[39] E.A. Lafayette, S.M.V. de Almeida, R.V. Cavalcanti Santos, J.F. de Oliveira, C. Amorim, R.M.F. da Silva, M. Pitta, I.D.R. Pitta, R.O. de Moura, L.B. de Carvalho Junior, M.J.B. de Melo Rego, M. de Lima, Synthesis of novel indole derivatives as promising DNA-binding agents and evaluation of antitumor and antitopoisomerase I activities, Eur. J. Med. Chem. 136 (2017) 511–522, https://doi.org/10.1016/j.ejmech.2017.05.012.
[40] Q. Wang, W. Li, A. Liu, B. Zhang, F. Gao, S. Li, X. Liao, Binding and photocleavage of a neutral nickel(II) bis(hydrogen pyridine-2,6-dicarboxylato) complex to DNA, J. Mol. Struct. 985 (2–3) (2011) 129–133, https://doi.org/10.1016/j.molstruc.2010.10.032.
[41] G.J. Chen, X. Qiao, P.Q. Qiao, G.J. Xu, J.Y. Xu, J.L. Tian, W. Gu, X. Liu, S.P. Yan, Synthesis, DNA binding, photo-induced DNA cleavage, cytotoxicity and apoptosis studies of copper(II) complexes, J. Inorg. Biochem. 105 (2) (2011) 119–126, https://doi.org/10.1016/j.jinorgbio.2010.11.008.
[42] K. Amirbekyan, N. Duchemin, E. Benedetti, R. Joseph, A. Colon, S.A. Markarian, L. Bethge, S. Vonhoff, S. Klussmann, J. Cossy, J.-J. Vasseur, S. Arseniyadis, M. Smietana, Design, synthesis, and binding affinity evaluation of Hoechst 33258 derivatives for the development of sequence-specific DNA-based asymmetric catalysts, ACS Catal. 6 (5) (2016) 3096–3105, https://doi.org/10.1021/acscatal.6b00495.
[43] M.R. Duff, V.K. Mudhivarthi, C.V. Kumar, Rational design of anthracene-based DNA binders, J. Phys. Chem. B 113 (6) (2009) 1710–1721, https://doi.org/10.1021/jp807164f.
[44] B. Jana, S. Senapati, D. Ghosh, D. Bose, N. Chattopadhyay, Spectroscopic exploration of mode of binding of ctDNA with 3-hydroxyflavone: a contrast to the mode of binding with flavonoids having additional hydroxyl groups, J. Phys. Chem. B 116 (1) (2012) 639–645, https://doi.org/10.1021/jp2094824.
[45] C.V. Kumar, R.S. Turner, E.H. Asuncion, Groove binding of a styrylcyanine dye to the DNA double helix: the salt effect, J. Photochem. Photobiol. A 74 (2) (1993) 231–238 https://doi.org/https://doi.org/10.1016/1010-6030(93)80121-O.
[46] L. Ma, J. Wang, Y. Zhang, Probing the Characterization of the Interaction of Aflatoxins B1 and G1 with Calf Thymus DNA In Vitro, Toxins (Basel) 9(7) (2017), https://doi.org/10.3390/toxins9070209.
[47] T. Sarwar, S.U. Rehman, M.A. Husain, H.M. Ishqi, M. Tabish, Interaction of coumarin with calf thymus DNA: deciphering the mode of binding by in vitro studies, Int. J. Biol. Macromol. 73 (2015) 9–16, https://doi.org/10.1016/j.ijbiomac.2014.10.017.
[48] A. Saswati, S.P. Chakraborty, A.K. Dash, R. Panda, A. Acharyya, S. Biswas, S.K. Mukhopadhyay, A. Bhutia, Y.P. Crochet, M. Patil, R. Nethaji, Dinda, Synthesis, X-ray structure and in vitro cytotoxicity studies of Cu(I/II) complexes of thiosemicarbazone: special emphasis on their interactions with DNA, Dalton Trans. 44 (13) (2015) 6140–6157, https://doi.org/10.1039/c4dt03764b.
[49] R. Raj Kumar, M.K. Mohamed Subarkhan, R. Ramesh, Synthesis and structure of nickel(ii) thiocarboxamide complexes: effect of ligand substitutions on DNA/protein binding, antioxidant and cytotoxicity, RSC Adv. 5 (58) (2015) 46760–46773, https://doi.org/10.1039/c5ra06112a.
[50] N. Shahabadi, S. Mohammadi, Synthesis characterization and DNA interaction studies of a new Zn(II) complex containing different dinitrogen aromatic ligands, Bioinorg. Chem. Appl. 2012 (2012) 571913, , https://doi.org/10.1155/2012/571913.
[51] P.C. Dedon, Determination of binding mode: intercalation, Curr Protoc Nucleic Acid Chem Chapter 8 (2001) Unit 8 1, https://doi.org/10.1002/0471142700.nc0801s00.
[52] Y. Wei, L.-H. Guo, Binding interaction between polycyclic aromatic compounds and DNA by fluorescence displacement method, Environ. Toxicol. Chem. 28 (5) (2009) 940–945 https://doi.org/doi:10.1897/08-394.1.
[53] L. Kapicak, E.J. Gabbay, Effect of aromatic cations on the tertiary structure of deoxyribonucleic acid, J. Am. Chem. Soc. 97 (2) (1975) 403–408.
[54] L.-M. Chen, J. Liu, J.-C. Chen, S. Shi, C.-P. Tan, K.-C. Zheng, L.-N. Ji, Experimental and theoretical studies on the DNA-binding and spectral properties of water-soluble complex [Ru(MeIm)4(dpq)]2+, J. Mol. Struct. 881 (1) (2008) 156–166 https://doi.org/https://doi.org/10.1016/j.molstruc.2007.09.010.
[55] N. Holmgaard List, J. Knoops, J. Rubio-Magnieto, J. Ide, D. Beljonne, P. Norman, M. Surin, M. Linares, Origin of DNA-induced circular dichroism in a minor-groove Binder, J. Am. Chem. Soc. 139 (42) (2017) 14947–14953, https://doi.org/10.1021/jacs.7b05994.
[56] M.S. Ali, M.A. Farah, H.A. Al-Lohedan, K.M. Al-Anazi, Comprehensive exploration of the anticancer activities of procaine and its binding with calf thymus DNA: a multi spectroscopic and molecular modelling study, RSC Adv. 8 (17) (2018) 9083–9093, https://doi.org/10.1039/c7ra13647a.
[57] S. Xuan, Z. Meng, X. Wu, J.-R. Wong, G. Devi, E.K.L. Yeow, F. Shao, Efficient DNA-mediated electron transport in ionic liquids, ACS Sustain. Chem. Eng. 4 (12) (2016) 6703–6711, https://doi.org/10.1021/acssuschemeng.6b01605.
[58] E. Kikuta, S. Aoki, E. Kimura, New potent agents binding to a poly(dT) sequence in double-stranded DNA: bis(Zn(2+)-cyclen) and tris(Zn(2+)-cyclen) complexes, J. Biol. Inorg. Chem. 7 (4–5) (2002) 473–482, https://doi.org/10.1007/s00775-001-0322-2.
[59] P.O. Vardevanyan, A.P. Antonyan, M.A. Parsadanyan, M.A. Shahinyan, L.A. Hambardzumyan, M.A. Torosyan, A.T. Karapetian, The influence of GC/AT composition on intercalating and semi-intercalating binding of ethidium bromide to DNA, J. Braz. Chem. Soc. 23 (2012) 2016–2020.
[60] S. Varadarajan, D. Shah, P. Dande, S. Settles, F.X. Chen, G. Fronza, B. Gold, DNA damage and cytotoxicity induced by minor groove binding methyl sulfonate esters, Biochemistry 42 (48) (2003) 14318–14327, https://doi.org/10.1021/bi0353272.
[61] B.C. Bales, T. Kodama, Y.N. Weledji, M. Pitie, B. Meunier, M.M. Greenberg, Mechanistic studies on DNA damage by minor groove binding copper-phenanthroline conjugates, Nucleic Acids Res. 33 (16) (2005) 5371–5379, https://doi.org/10.1093/nar/gki856.
[62] R. Ashraf, M. Hamidullah, P. Hasanain, M. Pandey, L.R. Maheshwari, M.Q. Singh, R. Siddiqui, K.V. Konwar, J. Sarkar Sashidhara, Coumarin-chalcone hybrid instigates DNA damage by minor groove binding and stabilizes p53 through post translational modifications, Sci. Rep. 7 (2017) 45287, https://doi.org/10.1038/srep45287.
[63] K.S. Saini, Hamidullah, R. Ashraf, D. Mandalapu, S. Das, M.Q. Siddiqui, S. Dwivedi, J. Sarkar, V.L. Sharma, R. Konwar, New orally active DNA minor groove binding small molecule CT-1 acts against breast cancer by targeting tumor DNA damage leading to p53-dependent apoptosis, Mol. Carcinog. 56 (4) (2017) 1266–1280, https://doi.org/10.1002/mc.22588.
[64] W.P. Roos, B. Kaina, DNA damage-induced cell death by apoptosis, Trends Mol.

Med. 12 (9) (2006) 440–450, https://doi.org/10.1016/j.molmed.2006.07.007.
[65] X. Zhang, S.C. Zhang, D. Sun, J. Hu, A. Wali, H. Pass, F. Fernandez-Madrid, M.R. Harbut, N. Tang, New insight into the molecular mechanisms of the biological effects of DNA minor groove binders, PLoS One 6 (10) (2011) e25822, , https://doi.org/10.1371/journal.pone.0025822.
[66] M. Hegde, K.S. Sharath Kumar, E. Thomas, H. Ananda, S.C. Raghavan, K.S. Rangappa, A novel benzimidazole derivative binds to the DNA minor groove and induces apoptosis in leukemic cells, RSC Adv. 5 (113) (2015) 93194–93208, https://doi.org/10.1039/c5ra16605e.
[67] D.J. Wong, L. Robert, M.S. Atefi, A. Lassen, G. Avarappatt, M. Cerniglia, E. Avramis, J. Tsoi, D. Foulad, T.G. Graeber, B. Comin-Anduix, A. Samatar, R.S. Lo, A. Ribas, Antitumor activity of the ERK inhibitor SCH772984 [corrected] against BRAF mutant, NRAS mutant and wild-type melanoma, Mol. Cancer 13 (2014) 194, https://doi.org/10.1186/1476-4598-13-194.
[68] A.A. Hassan, A.A. Aly, K.M.A. El-Shaieb, T.M.I. Bedair, S. Bräse, A.B. Brown, Synthesis of Thiazolidin-4-ones from Substituted (Ylidene) hydrazinecarbothioamides and Dimethyl Acetylenedicarboxylate, J. Heterocycl. Chem. 51 (3) (2014) 674–682, https://doi.org/10.1002/jhet.1642.
[69] A.A. Hassan, A.M. Nour El-Din, F.F. Abdel-Latif, S.M. Mostafa, S. Bräse, Formation of dioxospiroindene[1,3]thiazine and thioxoindeno[2,1-d]imidazolone derivatives from alkenylidene-hydrazinecarbothioamides, Chem. Papers 66 (4) (2012) 295–303, https://doi.org/10.2478/s11696-012-0145-3.
[70] A.A. Hassan, N.K. Mohamed, M.M. Makhlouf, S. Bräse, M. Nieger, H. Hopf, (Hex-2-en-ylidene)-N-Substituted Hydrazinecarbothioamides and 2,3-Dichloro-1,4-naphthoquinone: Nucleophilic Substitution Reactions and Synthesis of Naphtho[2,3-f][1,3,4]thiadiazepines and Naphtho[2,3-d]thiazoles, Synthesis 48 (18) (2016) 3134–3140, https://doi.org/10.1055/s-0035-1562133.
[71] G.M. Sheldrick, A short history of SHELX, Acta Crystallogr. A 64 (Pt 1) (2008) 112–122, https://doi.org/10.1107/S0108767307043930.
[72] G.M. Sheldrick, SHELXT – integrated space-group and crystal-structure determination, Acta Crystallogr. A Found Adv. 71 (Pt 1) (2015) 3–8, https://doi.org/10.1107/S2053273314026370.